

Comprehensive Signal Quality Evaluation of a Wearable Textile ECG Garment: A Sex-Balanced Study

Maximilian P. Oppelt, Tobias S. Zech, Sarah H. Lorenz, Laurenz Ottmann, Jan Steffan,
Bjoern M. Eskofier, Nadine R. Lang-Richter and Norman Pfeiffer

Abstract—We introduce a novel wearable textile-garment featuring an innovative electrode placement aimed at minimizing noise and motion artifacts, thereby enhancing signal fidelity in Electrocardiography (ECG) recordings. We present a comprehensive, sex-balanced evaluation involving 15 healthy males and 15 healthy female participants to ensure the device’s suitability across anatomical and physiological variations. The assessment framework encompasses distinct evaluation approaches: quantitative signal quality indices to objectively benchmark device performance; rhythm-based analyses of physiological parameters such as heart rate (HR) and heart rate variability (HRV); machine learning classification tasks to assess application-relevant predictive utility; morphological analysis of ECG features including amplitude and interval parameters; and investigations of the effects of electrode projection angle given by the textile / body shape, with all analyses stratified by sex to elucidate sex-specific influences. Evaluations were conducted across various activity phases representing real-world conditions. The results demonstrate that the textile system achieves signal quality highly concordant with reference devices in both rhythm and morphological analyses, exhibits robust classification performance, and enables identification of key sex-specific determinants affecting signal acquisition. These findings underscore the practical viability of textile-based ECG garments for physiological monitoring as well as psychophysiological state detection. Moreover, we identify the importance of incorporating sex-specific design considerations to ensure equitable and reliable cardiac diagnostics in wearable health technologies.

Index Terms—Electrocardiography, Garments, Machine Learning, Signal Quality, Smart Textiles, Wearables

I. INTRODUCTION

This is a preprint of a manuscript submitted for publication. It has not yet been peer-reviewed, and the final version may differ.

The authors acknowledge the funding by the EU TEF-Health project which is part of the Digital Europe Program of the EU (DIGITAL-2022-CLOUD-AI-02-TEFHEALTH).

M. P. Oppelt (Main Contributing Author) is Senior Scientist at the Department Digital Health and Analytics, Fraunhofer IIS, Fraunhofer Institute for Integrated Circuits IIS, 91058 Erlangen, Germany and with the Department Artificial Intelligence in Biomedical Engineering, Friedrich-Alexander-University Erlangen Nuremberg, 91052 Erlangen, Germany (*Corresponding e-mail: maximilian.oppelt@iis.fraunhofer.de*)

Bjoern M. Eskofier is Professor at the Department Artificial Intelligence in Biomedical Engineering, Friedrich-Alexander-University Erlangen Nuremberg, 91052 Erlangen and Principal Investigator for Translational Digital Health Group at Institute of AI for Health Helmholtz Zentrum München, 85764 Munich, Germany

T. Zech, S.H. Lorenz, L. Ottmann, J. Steffan, N.R. Lang-Richter and N. Pfeiffer are with the Department Digital Health and Analytics, Fraunhofer IIS, Fraunhofer Institute for Integrated Circuits IIS, 91058 Erlangen, Germany

ELECTROCARDIOGRAPHIC recordings serve as a fundamental diagnostic tool in modern medicine, providing invaluable noninvasive insights into the electrical activity of the heart and therefore the health of the cardiovascular system. Introduced by Willem Einthoven in the early 20th century, Electrocardiography (ECG) remains a cornerstone in clinical cardiology. Einthoven’s pioneering work laid the foundation for understanding the principles underlying ECG acquisition and interpretation [1], [2].

ECG signals are acquired through electrodes placed on the skin, capturing the electrical impulses generated by cardiac muscle de- and repolarization. These signals manifest as characteristic waves on the ECG tracing, reflecting the sequential activation of different regions of the heart [3].

In modern medicine, ECG is used in applications ranging from diagnosing cardiac arrhythmias [4] and ischemic heart disease [5] to monitoring patients during surgery [6] and assessing the effects of pharmacological interventions [7], [8]. Moreover, recent advancements in wearable devices have expanded ECG applications beyond traditional cardiology, enabling emerging research in affective sensing [9] and stress detection during daily activities [10].

Each of these applications have domain specific requirements regarding the quality of the ECG signal, the duration of the recording, usability, accessibility, the comfort of the patient and costs. While the traditional approach of using Ag/AgCl gel electrodes provides reliable signal quality, it also presents several limitations. These include the risk of skin irritation [11], [12], the limitation that only trained professionals are able to correctly apply the adhesive electrodes at specific anatomical locations [13], and restricted freedom of movement imposed on patients during daily activities by the presence of electrodes and connecting wires.

Recent advances in wearable technology have addressed specific challenges in health monitoring applications. Devices such as smartwatches [14] and smart rings [15] utilize Photoplethysmography (PPG) to measure heart rate (HR) and heart rate variability (HRV), thereby enabling applications such as activity tracking [16] and stress monitoring [17]. Despite their utility, these devices have limited accuracy in capturing the precise timing of heartbeats, as they measure the mechanical pulse of blood flow rather than the heart’s electrical activity. Consequently, their diagnostic capabilities are restricted, particularly for conditions such as ischemic heart disease or conduction disorders, as well as for obtaining

accurate HRV parameter estimates, all of which require precise beat segmentation. Furthermore, their measurements are susceptible to noise arising from individual patient characteristics such as skin tone, weight, age, and gender as well as physiological factors including blood pressure and temperature, and external influences like ambient lighting conditions [18]. Another category of devices, such as the Apple Watch [19], is capable of recording brief segments of ECG waveforms and can automatically detect arrhythmias [20], [21]. Similarly, systems like AliveCor [22], [23] are utilized to assess morphological changes during pharmacological studies [24]. Smart textiles represent a unique class of wearable devices that can continuously record the heart's electrical activity over extended periods [25]. Unlike conventional wearables, smart textiles offer enhanced comfort and freedom of movement, enabling unobtrusive and continuous ECG monitoring during daily activities. This is achieved by seamlessly integrating flexible dry electrodes into the garment itself, thereby further enhancing wearer comfort [26]–[28]. Various research groups and device manufacturers have developed different materials for this purpose, like metal based contact surfaces [25], [29]–[33], conductive polymers [25], [32]–[36] and carbon materials [25], [35], [37], [38]. These conductive materials are integrated into the textile using various fabrication techniques: Embroideries, knittings, sewings and weavings are used to classically integrate yarns [32], [53]–[55]. Others have printed [56], electrostatically flocked [57], or dip coated [37] conductive materials onto the textiles. Table I summarizes several studies that have introduced novel materials and integration techniques for textile electrodes. These efforts seek to optimize the signal-to-noise ratio, lower skin-electrode impedance, reduce motion artifacts through robust and stable skin-electrode contact, increase durability, including machine washability and maintain biocompatibility.

Significant differences exist in physiological parameters between male and female ECG recordings. For instance, women typically exhibit a higher HR, a lower ST-segment, and a reduced T-wave amplitude compared to men [58], [59]. Other anatomical factors, including variations in chest shape affecting electrode placement and differences in heart size [60], can result in ambiguous recordings, potentially leading to invalid diagnoses with certain electrode positions [61]. When developing a new system intended for use by both sexes, it is crucial to evaluate the system with a diverse study population. This ensures that the system is not biased and, as a result, can provide valid diagnostics [62], [63].

A primary motivation for developing new wearable sensor technology is to enable the continuous acquisition of high-quality ECG recordings. However, current research in this field reveals several limitations, including small sample sizes, study populations restricted to a single gender (typically male), and evaluation methodologies that focus exclusively on electrode materials rather than assessing the signal quality of the entire wearable system. These shortcomings, as detailed in Table I, give rise to two primary research questions: **RQ1)** How does a wearable ECG textile with integrated dry silicone electrodes perform in accurately measuring ECG parameters like HR, HRV, and morphology compared to a medical-grade gold-

standard Holter ECG during different activities like sedentary tasks versus dynamic movements like walking or running? **RQ2)** To what degree does the structural design of the textile-based ECG system influence the quality of recorded signals, particularly in regard to addressing potential gender-related disparities in cardiac diagnostics?

II. METHODS

To evaluate the functionality and accuracy of our textile-based ECG device, participants simultaneously wore our wearable textile shirt with integrated dry electrodes, as well as two reference systems representing the current gold standard, each employing Ag/AgCl electrodes. The textile incorporates four



Fig. 1: Wearable textile with integrated electrodes and connectors: rear view with button connectors (left), interior wiring (middle), and close-up of flexible dry electrode (right).

electrodes Left Arm (LA), Right Arm (RA), Left Leg (LL), and Right Leg (RL) providing three bipolar leads (two directly measured and one calculated), corresponding to modified Einthoven leads recorded at the torso. Figure 1 provides an overview of the garment with integrated electrodes and connections. The fourth electrode serves as the neutral electrode. Flexible electrodes entail a multilayer structure comprising 78% polyamide and 22% elastomer stretch-tricot, metal-plated with silver ($26.9 \pm 1\%$), topped off by a conductive silicone sheet. This composition ensures durability and low surface resistance, while its stretch properties provide comfort during wear. The electrode cables are seamlessly integrated into the textile and routed to a central hub positioned at the back of the subject's neck, where the connectors are located. These connectors feature buttons to which the hardware can be attached. The electronics are responsible for digitizing the signal using a ADS1293 (Texas Instruments, USA) analog front-end. The data storage on an SD card is handled by the microcontroller nRF52840 (Nordic Semiconductor, Norway). During setup, the live signal is monitored via Bluetooth transmission, while recorded data stored on the SD card is used for subsequent evaluation, ensuring data consistency without potential loss of wireless connections. As reference systems, we used two commercially available medical devices: the BTL (BTL GmbH, Dornstadt, Germany) BT-08 Holter monitor and the Bittium (Bittium Corp., Oulu, Finland) Faros 180. Both devices are approved for medical use and were operated with Ag/AgCl wet electrodes.

A. Study Population

The study population consists of 30 subjects, with 15 males and 15 females. The minimal age is 21, the maximal age is 60, and the mean age is 30.2 with a standard deviation of 8.4. The height distribution for males and females, as well as

TABLE I: Related work on textile-based ECG monitoring with the number of subjects, electrode setup, protocol, reference system, and selected quality assessment, sorted by date of publication. (F: Female, M: Male, U: Unknown)

Ref.	Study Population	Electrodes (el) Channels (ch.)	Protocol	Reference System	Quality Assessment
[39]	5 (5M), healthy	3 el. (RA, LA, LL), 2 ch. (mod. Einthoven)	standing, sitting (relaxed)	Biopac MP150 (Ag/AgCl)	R-Peak detection rate (estimated/observed)
[40]	40 (40M), cardiovascular diseases	2 (V5, V5R)	20 subjects (in bed), 20 subjects (mild exercise, cycloergometer, walking)	CL Delta / Fukuda Denshi DS 5700 (Ag/AgCl)	cardiologist rating (artifacts, morphological, rhythm), compute rule based rating
[41]	4 (4M), healthy	2 el. (chest belt), 1 ch. (custom)	standing, treadmill (4, 5, 6, 7 km/h)	Biopac MP150 (Ag/AgCl)	QRS delineation, sensitivity, accuracy, TP, FP, FN
[42]	12* (12U), unknown	3 el. (reference + 2 custom), 1 ch. (custom)	rest and unknown motion	Synmedic Ambu Blue (Ag/AgCl)	subjective rating
[34]	10 (10U), healthy	various (task dependent)	sitting, breathing, stairs, 2Hz step-up-down-exercise	-	QRS detection rate, RMSE
[43]	3 (3M), unknown	9 el (chest), 8 ch. (12 Mason-Likar)	lying, sitting, walking	Corscience Holter ECG BT12 (Ag/AgCl)	Bland-Altman, fiducial points, reference correlation
[44]	10 (10U), healthy	3 el (RA, RA, LL [†]), 1 ch. (mod. Lead I)	-	Unknown (Ag/AgCl)	R-peak amplitude and variations, SNR
[45]	4 (2M, 2F), healthy, minors	2 el. (chest), 1 ch. (custom)	resting, walking, running (12 km/h)	Cardiac Monitor Arm Band (Ag/AgCl)	visual inspection, HR, tachycardia/extra-systoles
[35]	1 (1U), healthy	3 el (LA, RA, LL), 1 ch. (mod. Lead I)	-	Analog Devices INA 2128 (Ag/AgCl)	visual inspection, reference signal correlation
[46]	1 (1F), healthy	3 el (chest band), 1 ch. (mod. Lead I)	sitting, walking	ADS1292ECG-FE (Ag/AgCl)	visual inspection, baseline wander, HF noise
[47]	4 (4U), healthy	3 el (LA, RA, LL), 1 ch. (mod. Lead I)	-	TMSI Proti7 (Ag/AgCl)	PSD, visual inspection, delineation
[36]	66 (47M, 19F*), healthy	2 el. (V5R, V5) 1 ch. (custom location)	supine rest, seated rest, trunk rotation, steps	Holter ECG Cardy 303 Pico+ (Ag/AgCl)	R-amplitude variations isoelectric line variations
[48]	1 (1F), healthy	3 el (LA, RA, LL), 1 ch. (Lead I)	resting	-	visual inspection, SNR
[38]	1 (1U), healthy	3 el. (LA, RA, LL), 1 ch. (mod. Lead I)	-	-	peak amplitude, SNR (PSD)
[49]	1 (1U), healthy	5 el. (LA, RA, LL, RL, V2), 4 ch. (mod. Einthoven, V2)	sitting, standing, walking, stair climbing	Texas Instruments ADS1298R (Ag/AgCl)	visual inspection
[50]	10 (10M), healthy	chest, unknown	relaxed, resting	-	PQRST delineation (recall, precision, F1)
[26]	1 (1U), healthy	3 el. (LA, RA, LL), 1 ch. (mod. Lead I)	resting	-	peak amplitude, pSQI, BasSQI
[51]	13 (6M, 7F), healthy	3 el. (LA, RA, LL, RL) 2 ch. (mod. Einthoven)	standing, treadmill, <i>n</i> -back task	Bittium Faros 360 NeXus-10 MKII Polar RS800 Multi SOMNOTouch NIBP	morphological, HR
[52]	30 (16M, 14F), healthy	2 el., 1 ch.	activity during daily living (unspecified)	3-lead holter monitor	subjective, R-R interval comparison
Ours	30 (15M, 15F), healthy	4 el. (LA, RA, LL, RL) 2 ch. (mod. Einthoven)	lying, sitting, walking, running	Bittium Faros 180 & BTL-08 Holter H600 (Ag/AgCl)	

* Female subjects wore a different type of garment (bra instead of shirt) and electrode setup.

[†] Ag/AgCl electrode as a reference electrode.

the weight distribution, is 181.7 ± 5.1 cm, 168.2 ± 6.8 cm and 84.7 ± 11.3 kg, 60.7 ± 7.4 kg respectively. We measured the under chest girth according to the ISO 8559 [64] standard. The lower chest girth is 93.9 ± 7.5 cm and 75.9 ± 4.6 cm for males and females respectively. All subjects participated voluntarily, had no known cardiovascular disease and were not taking any medication, except oral contraceptives, that could influence the ECG signal. The study was conducted in accordance with the Declaration of Helsinki and was approved by the Ethics Committee of Friedrich-Alexander-University Erlangen-Nuremberg (65_21 B, approved on 16.03.2021).

B. Measurement Locations and Reference Systems

Since Einthoven introduced the three standard limb leads, several modifications have been made to improve the prac-

ticality of lead placement. For example, during treadmill ECG exercise, electrodes are attached to the back to reduce movement artifacts. In mobile Holter systems, the electrodes are usually placed on the torso in the direction of the standard Einthoven limb leads to allow for greater freedom of movement. In our reference systems, the upper electrodes were mounted along the anterior axillary line (over the bone) at the level of the clavicle, while the lower electrodes were placed outside the anterior axillary line at the end of the ninth costal cartilage. For the BTL five-lead system, the precordial electrode was positioned at the fourth intercostal space on the right margin of the sternum (lead V1). This electrode placement was selected because it is a common scheme for Holter monitors and provides sufficient space to accommodate the textile system. The textile electrodes are positioned closer



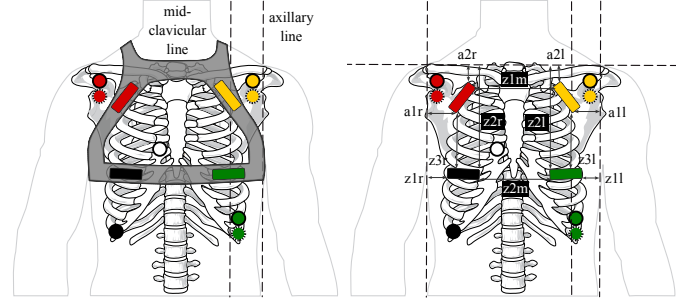
(a) Subject wearing the garment with integrated and reference electrodes. (b) System overview of the wearable with adjustable hook-and-loop fastener.

Fig. 2: Male subject wearing garment, showing reference electrode placement from both systems.

to the heart in alignment with the limb leads. The lower electrodes are placed at the fifth intercostal space on the anterior axillary line. These modifications are made to ensure a tight fit and minimize movement artifacts resulting from limb motion due to the greater distance. The garment was designed to ensure that the orientation of the electrodes closely aligns with natural physiological contours. Specifically, the upper electrodes were positioned at a 45-degree angle relative to the axillary line, while the lower electrodes were placed horizontally with a slight inward rotation shift towards the center. This configuration allows the electrodes to fit to the torso without protruding, thereby following the body's shape for optimal contact and comfort. The garment is designed with adjustable hook-and-loop fasteners positioned at both the upper and lower regions, enabling precise adaptation to various body shapes and ensuring a tight fit. To accommodate more substantial variations in body size, multiple garment sizes were produced in accordance with the DIN EN 13402-3:2017-12 standard, ranging from XS to XXL. The actual fit of the garment and the positioning of the hook-and-loop fasteners varies according to individual body shape, which may, in turn, affect the placement of the electrodes. To systematically assess electrode positioning, we measured several key distances, as illustrated in Figure 3a and Figure 3b. These figures depict the electrode locations for both the reference and textile systems, as well as the measured distances between the wearable electrodes and relevant anatomical landmarks. This approach enabled us to evaluate electrode positioning and analyze the impact on the anatomical projections.

C. Study Protocol

The study protocol comprised a series of four-minute tasks, beginning with an initial seated resting phase, followed by an n-back working memory task. In the n-back task, participants were presented with a sequence of stimuli and asked to indicate whether the current stimulus matched the one presented n steps before, thereby inducing a state of high cognitive load [65]. Subsequently, participants completed a range of physical tasks presented in randomized order: standing motionless in an upright posture; walking at a moderate pace (up to 5 km/h) with speed adjustments allowed for comfort; running at a brisker pace (up to 10 km/h) with speed modified for individual fitness and body characteristics; cycling on a



(a) Reference system electrodes (b) Locations of the reference electrodes positioned at modified Einthoven electrodes and the textile, illustrating the spatial relationship between the textile electrode location, with the textile electrodes and the shaded garment area.

Fig. 3: Electrode locations, fit and garment overview.

stationary bike at a target speed of 20 km/h, with adjustments permitted; and lying down in four different positions right side, left side, back, and prone position each for four minutes. The protocol concluded with a final four-minute seated period. Throughout, procedures were tailored to ensure participant safety and comfort while preserving experimental rigor.

D. Signal Quality Evaluation

In this study, we conduct signal quality evaluations without the use of human annotation or subjective feedback by domain experts. We assess the signal quality from multiple perspectives, each addressing distinct properties of the acquired signals. Signal quality measures, commonly employed by related literature, are extracted to compare devices during identical physical activity types. Additionally, physiological features based on rhythmic patterns, are extracted and compared between devices to further assess the integrity of the signals. We are accompanying this rhythm based evaluation by conducting a statistical evaluation of beat-detection performance. Morphological features, which hold significant clinical and pharmaceutical relevance, are also examined in this study. Specifically, we analyze features such as QT intervals, commonly assessed in pharmaceutical research, as well as amplitude markers associated with ventricular de- and repolarization. These amplitude markers are frequently utilized in clinical practice, for instance, in the detection of cardiac ischemia. Finally, we consider morphological changes that may intrinsically result from alternate electrode placement, acknowledging that such variations can influence the overall signal characteristics. This multifaceted evaluation strategy ensures a robust and objective assessment of signal quality. Initial preprocessing involves signal filtering, followed by segmentation procedures, including R-peak detection and fiducial point delineation. Detailed descriptions of these methods are provided in the Supplementary Material to ensure reproducibility while maintaining focus on the main research objectives.

1) *Signal Quality Indices*: We utilize Signal Quality Indices (SQIs) to assess each acquisition device individually. These SQIs are then compared across devices and tasks.

TABLE II: SQIs for ECG signals used in this study with references and a short description.

Ref.	Name	Description
[66]	sSQI	Skewness of the signal
[66]	kSQI	Kurtosis of the signal
[67]	pSQI	Relative power in the QRS complex $\int_{5Hz}^{15Hz} P(f)df / \int_{5Hz}^{40Hz} P(f)df$
[69]	cSQI	Regularity of RR intervals
[68]	qSQI	Matching degree of R peak detection (Detectors: [70] and [71])
[51]	morphSQI	Morphological SQI based on weighted cardiac cycle median deviation
Ours	vmSQI	Mean absolute distance of complexes to the median complex.

Previous studies [51], [66]–[68] introduced these indices for evaluating the quality of ECG signals. Table II presents the names, descriptions, and corresponding references for each Signal Quality Index (SQI). These indices capture multiple dimensions of signal quality, including morphological characteristics, spectral content, and measures of signal regularity. We calculate the SQIs for all leads and compare them across different phases. Previous studies have attempted to establish thresholds based on heuristic assumptions or trained classifiers using expert annotations on multiple SQIs. However, because these heuristics and classifiers are typically tailored to specific tasks and rely on subjective ECG quality assessments, we calculate SQIs to enable an objective comparison between different acquisition devices.

2) *Rhythmic Based Evaluation*: The second approach centers on the extraction and evaluation of widely recognized features associated with rhythmic physiological changes, specifically HR and HRV. In line with our initial methodology, we systematically compare these features across multiple acquisition devices, focusing on core parameters such as HR, the Root Mean Square of Successive Differences (RMSSD), the Standard Deviation of RR-Intervals (SDNN), and the High Frequency (HF) and Low Frequency (LF) spectral components. These metrics are extensively utilized in clinical contexts to assess autonomic function and cardiovascular health [72]. Given that the accurate estimation of these parameters depends on the reliable detection of heartbeats, typically achieved by identifying R-peaks in the ECG signal, we conduct a focused evaluation of R-peak detection performance. Specifically, we evaluate detection quality across three distinct devices by selecting ECG channel positions analogous to lead II, which is commonly employed in peak detection tasks [73]. The classification of detection events is illustrated in Figure 4, which provides a visual summary of typical signal artifacts and detection errors encountered during an active recording session. The figure highlights various categories of errors, including missed detections and invalid detections across different device channels. Notably, the depicted interval exhibits considerable movement and muscle noise artifacts. To comprehensively assess detection performance, we compare a reference device with the textile-based system across both male and female participants and throughout all experimental phases, accompanied by evaluating the reference devices with

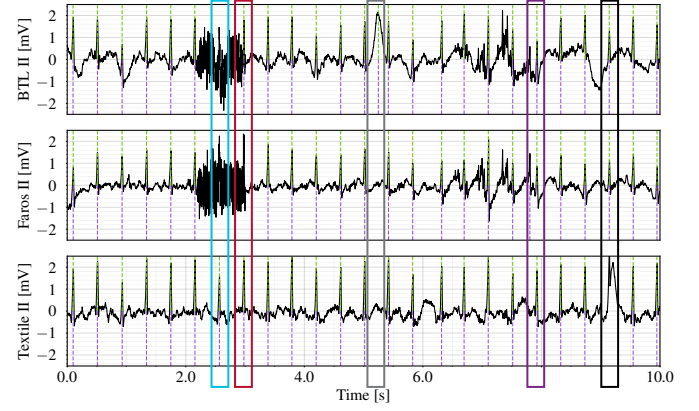


Fig. 4: Noisy data over time during an active session, showing signal artifacts and detection errors. Missed detections are marked for BTL and Faros II (blue), Faros II (red), and Textile II (black); invalid detections in BTL II (grey); and both invalid and missed detections in Faros II (purple). Movement and muscle noise are visible throughout. Dotted lines indicate detection results from the Hamilton (green) [74] and Rodrigues (purple) [71] detectors.

each other. Both the BTL and Faros systems utilize Ag/AgCl electrodes positioned in proximity to the body, thereby providing a robust reference measurement. To further elucidate the influence of signal projection, we report hit, miss, and false alarm rates of the lead I and V1 to the reference system Lead II. This analysis underscores the impact of electrode positioning and channel selection on detection fidelity. To quantitatively compare the raw detection rates observed across different devices, we estimate the parameters of a Dirichlet distribution using Maximum Likelihood Estimation (MLE) [75]. Probabilistic modeling of detection events enables the performance of different devices to be represented by the parameter vector α , facilitating a robust comparison between detection events of different devices.

3) *Classification*: We trained classifiers on surrogate tasks to assess the predictive performance for common ECG applications using different acquisition devices. To accomplish this, we introduce two commonly evaluated tasks in ECG signal processing and train classifiers on the ECG signals. Both tasks employ rhythmic features, consistent with established applications in physiological signal processing of ECG signals. The HRV features include time-domain measures, such as the SDNN and the Standard Deviation of the Successive Differences (SDSD). Frequency-domain features are also utilized, specifically the low-frequency (0.04–0.15 Hz) and high-frequency (0.15–0.4 Hz) components, as well as the ratio of high-to-low frequency spectral components (HF/LF). In addition, features derived from the graphical Poincaré plot the SD1 and SD2 components and their ratio (SD1/SD2) are incorporated. All features are extracted from lead II. Our activity recognition task is formulated as a three-class problem using a balanced dataset comprising the classes *Active*, *Sitting*, and *Lying*. The *Active* class includes activities performed during cycloergometer use, treadmill running, and treadmill walking.

The *Sitting* class encompasses periods when the subject is sitting relaxed, watching a video, or participating in the n-back experiment. The *Lying* class captures instances where the subject is lying on their back, left side, or in prone position. The second machine learning task utilizes the same feature set as input, but is designed to distinguish between two classes reflecting different psycho-physiological states. The *Low* load class represents a condition where the subject is sitting upright at rest without any imposed task. In contrast, the *High* load class corresponds to the state in which the subject is engaged in solving the second level of the n-back test, a condition known to induce a high level of task load [9], [65]. We trained our models using lead II data from both the primary reference system and the textile-based system. Feature extraction was performed for each phase, followed by normalization via z-score transformation to achieve zero mean and unit standard deviation. For classification, we employed *XGBoost*, a model widely used in feature-based detection of psycho-physiological states [9]. The dataset was partitioned on a subject-wise basis using a 5x5 nested cross-validation scheme. We report the mean and standard error of the Area Under the Curve (AUC) and F_1 score for both tasks and devices.

4) *Morphological Comparison*: The morphological comparison of ECG recordings obtained simultaneously from two devices, each employing distinct electrode placements, presents inherent challenges due to the differing spatial projections resulting from the cardiac electrical activity. Specifically, the orientation and placement of electrodes significantly affect the measured signals, as each device records the cardiac electrical field from a distinct spatial perspective. Integrating electrodes into a textile demands further adjustment of lead positions to fulfill both ergonomic requirements and the minimization of noise artifacts due to relative electrode-skin movement, as depicted in Figure 2. In addition, the use of the aforementioned silicon-based electrode material, in contrast to the Ag/AgCl wet electrodes used in the reference system, exhibits distinct characteristics with respect to modeling the skin-electrode interface [76], [77]. These modifications are essential to ensure user comfort and robust signal acquisition but, in turn, complicate direct morphological comparisons between signals derived from disparate lead configurations. Non-standard Einthoven placement of electrodes without detailed indication might cause diagnostic issues [78]. As an initial step in our morphological assessment, we extract commonly used fiducial points in ECG analysis and compute both interval- and amplitude-related measures. Specifically, we determine the amplitude from the isoelectric line to the R wave, the amplitude of the ST segment, the amplitude from the isoelectric line to the T wave, and the amplitude from the isoelectric line to the P wave. Additionally, we calculate the QT interval, representing the time duration from the onset of the Q wave to the end of the T wave, as well as the T-length, defined as the interval between T-onset and T-offset (extracted using tangents [79]), as shown in Figure 5. Direct projection or transformation of ECG signals between such configurations is nontrivial, as the inverse problem is ill-posed and affected by factors such as respiratory motion, the variable composition of intervening tissues (e.g., skin and fat layers), and, critically, the relative

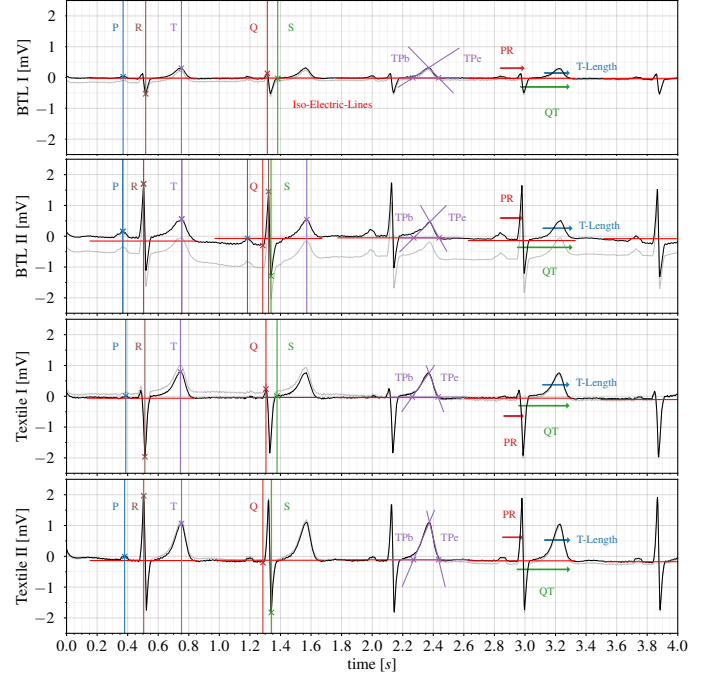


Fig. 5: Lead I/II for BTL and textile devices, showing fiducial points (PQRST), isoelectric line, comparison intervals, unfiltered (gray), and 0.67 Hz highpass-filtered (black) signals.

orientation of each electrode set with respect to the cardiac vector [80]. Recognizing these complexities, we approximate the correspondence between the two electrode systems as a transformation comprising rotation and linear scaling within the lead I/II plane. To formalize this, we frame the problem as a one-sided Procrustes analysis, where the objective is to optimally align the median complexes extracted from the textile-based recordings, denoted as $\mathbf{A} \in \mathbb{R}^{d \times n}$, to those from the reference BTL system, denoted as $\mathbf{B} \in \mathbb{R}^{d \times n}$, with $d = 2$ corresponding to leads I and II and n to the median complex sequence length. The transformation is modeled as a right-sided operation, with parameters determined by minimizing the squared Frobenius norm $\|\cdot\|_F^2$, as shown in Equation 1.

$$\min_{\{\mathbf{R} \mid \mathbf{R}^{-1} = \mathbf{R}^\dagger, |\mathbf{R}| = 1\}} \|\mathbf{A}\mathbf{R} - \mathbf{B}\|_F^2 \quad (1)$$

To enhance alignment, we first normalize the textile-based median complex \mathbf{A} to match the maximal amplitude observed in the reference system \mathbf{B} . Specifically, for each sample in both \mathbf{A} and \mathbf{B} , we compute the instantaneous magnitude across leads I and II as $|\mathbf{v}| = \sqrt{I^2 + II^2}$. We then determine the normalization constant s as the ratio of the maximum absolute magnitude in the reference system to that of the textile system, that is, $s = \max(|\mathbf{v}_B|) / \max(|\mathbf{v}_A|)$. The textile signals are subsequently scaled by this constant prior to transformation, ensuring that both datasets are on a comparable amplitude scale and thereby improving the robustness of the subsequent Procrustes alignment. To quantitatively assess the quality of alignment between the transformed textile-based and reference ECG signals, we employ three similarity measures: the squared Frobenius norm error, the Root Mean

Square Deviation (RMSD), and the cosine similarity. Upon determination of the optimal rotation parameters within the I/II plane, we further correlate these findings with individual anthropometric measurements to elucidate which physiological attributes most significantly influence the effects of altered electrode placement. This integrative approach not only enables rigorous morphological comparison between textile and reference ECG recordings but also advances our understanding of the anthropometric determinants impacting signal morphology under novel electrode configurations.

III. RESULTS

A. Comfort and Fit

The subjects were provided with appropriately sized garments, with size distribution as follows: among male participants, none wore size XS or XXL, while one wore size S, four wore size M, six wore size L, and four wore size XL. Among female participants, one wore size XS, ten wore size S, four wore size M, and none wore sizes L, XL, or XXL. The wearable garments were designed with a unisex sizing scheme. Participants were subsequently asked to assess their subjective comfort using a five-point Likert scale, ranging from 1 (very uncomfortable, barely tolerable, and highly disturbing) to 5 (very comfortable, such that the wearer forgot they were wearing the textile). The overall comfort ratings for male participants were distributed as follows: two rated the textiles as 2, six as 3, five as 4, and two as 5. For female participants, eight assigned a rating of 3, six a rating of 4, and one a rating of 5.

B. Signal Quality

1) *SQIs*: For *cSQI*, the lowest values are observed in BTL, Faros, and Textile Lead II. Other leads not only exhibit higher values during lying and sitting phases but also increase during more rigorous activities, such as treadmill running. Given that *cSQI* is primarily based on RR interval detection, these findings suggest that the projection of Lead II is optimal for R-peak detection, with device-specific differences playing a minor role in this particular SQI. The *ksQI* highlights the pronounced effects of intense activities, with the lowest values recorded during cycloergometer and treadmill running phases. *morphSQI* reveals the most pronounced changes across all SQIs for the textile electrode. This observation underscores that the morphology of individual heart complexes can differ from the surrounding signal, potentially due to baseline wander or other low-frequency variations. Regarding *pSQI*, although the median values remain similar across all phases, leads I and V1 exhibit greater variance compared to lead II. This further emphasizes the impact of lead placement, which alters the ratio between low and high frequency components in the QRS complexes. The *qSQI* demonstrates lower values during lying phases, while sitting and standing phases yield the highest values. This index reflects the degree of concordance between two R-peak detectors, while lead II of all systems generally has higher values compared to lead I and lead V1. *sSQI* shows that leads I and V1 consistently yield lower values than lead II across all devices. For *vmSQI*, variance and changes

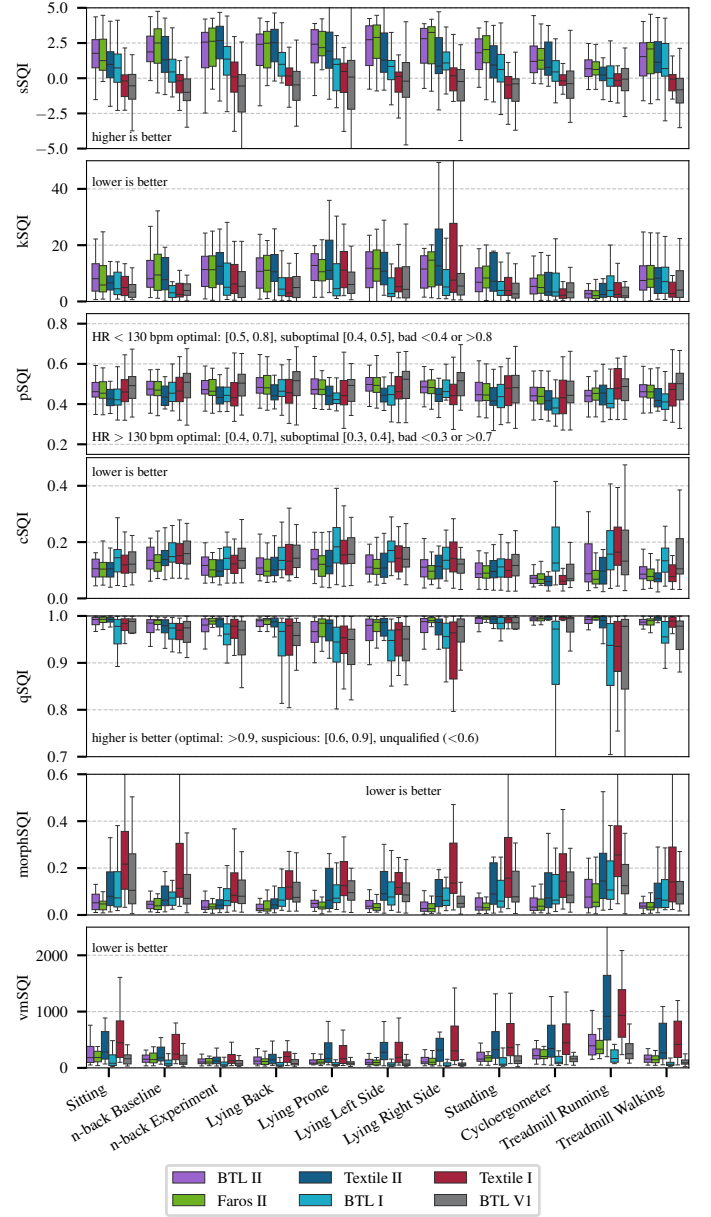


Fig. 6: SQIs for all recorded leads and devices during different phases of the study with indication of better signal quality according to original publication.

are generally minimal across all leads, except during running and walking phases, where increased variance is observed. In summary, while several parameters suggest that lead II performs comparably to the reference systems even at varying activity intensities, the statistical evaluation alone does not provide a comprehensive assessment. Lead placement exerts a more significant influence on the computed SQIs than artifacts such as baseline wander, muscle noise, or movement artifacts. Therefore, a thorough evaluation should prioritize practical applicability and intended use rather than relying solely on statistical features.

2) *Physiological Parameters*: Mean HR, as well as HRV indices RMSSD and SDNN, together with the LF/HF spectral ratio, are widely employed in fitness and psychophysiological assessments. To evaluate the agreement between devices,

we present these parameters using Bland-Altman plots, as illustrated in Figure 7. The results for HR and time-domain HRV measures show close agreement between devices for the majority of measurements. The observed outliers are typically attributable to errors in R-peak detection. Specifically, the mean difference is -0.38 for HR, -0.93 for RMSSD, -0.86 for SDNN, and -0.06 for the LF/HF ratio, indicating a high level of concordance between the measurement devices. No

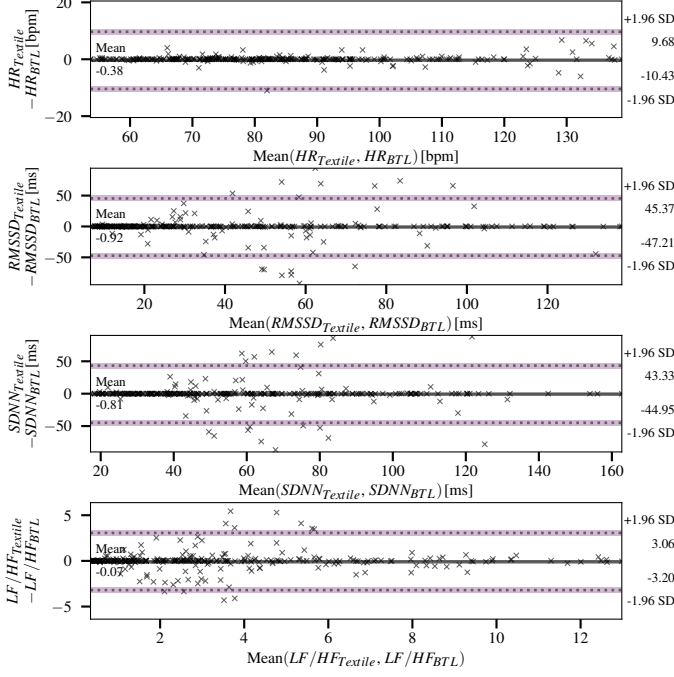


Fig. 7: Bland-Altman plots comparing BTL reference and textile ECG systems for HR, RMSSD, SDNN, and HF/LF.

systematic errors are observed, such as higher values resulting in greater deviations between the two devices. Visualizations in our supplementary material, reveal a high correlation of up to $R = 0.93$, with minor reductions in correlation primarily attributable to R-peak detection errors. We present the hit rate, miss rate, and false alarm rate for all leads, compared to the reference device, across all phases in Table III, separated by sex. The results indicate that the textile performs equally well for both female and male subjects, achieving a hit rate of 0.95 ± 0.10 for females and 0.95 ± 0.12 for males. This performance is comparable to that of the secondary reference device, Faros, which demonstrates hit rates of 0.96 ± 0.07 for females and 0.97 ± 0.04 for males. Additionally, we report the R-peak detection performance for lead I, showing lower performance for females compared to males, indicating a strong impact of RA/LA electrode placement on R-peak detectability. As our recordings were neither annotated nor manually cleaned to remove noisy segments, the reference device is also affected by reduced detection performance. The Faros reference device, based on the same technology, was positioned in close-proximity to the BTL leads. Table IV presents the intersecting R-peak detections among the three devices. Notably, 0.941 of all R-peak events are detected by all devices, indicating a substantial agreement. Conversely,

TABLE III: R-peak detection performance by lead and sex, showing mean hit, miss, and false alarm rates.

		Hit	Miss	False Alarm
Female	BTL I	0.89 ± 0.17	0.04 ± 0.08	0.07 ± 0.09
	BTL V1	0.80 ± 0.30	0.09 ± 0.15	0.11 ± 0.15
	Textile I	0.74 ± 0.34	0.12 ± 0.17	0.14 ± 0.18
	Textile II	0.95 ± 0.10	0.02 ± 0.05	0.03 ± 0.07
	Faros II	0.96 ± 0.07	0.02 ± 0.03	0.02 ± 0.05
Male	BTL I	0.94 ± 0.11	0.02 ± 0.04	0.04 ± 0.07
	BTL V1	0.76 ± 0.32	0.11 ± 0.16	0.13 ± 0.16
	Textile I	0.90 ± 0.18	0.04 ± 0.08	0.06 ± 0.11
	Textile II	0.95 ± 0.12	0.02 ± 0.04	0.03 ± 0.08
	Faros II	0.97 ± 0.04	0.01 ± 0.01	0.02 ± 0.03

0.022 of events are detected by both reference systems but not by the textile electrode, providing a reliable estimate of the textile's miss rate. Additionally, 0.007 of events are not detected by either the Faros or BTL device, which reflects potential false positives by the textile electrode. When interpreting these results, it is essential to recognize that the reference systems were likely exposed to noise sources similar to those affecting the textile device. Both reference systems utilized Ag/AgCl electrodes, which were mounted in close proximity, closer than the textile electrodes, and connected by cables routed together. This configuration increased their susceptibility to similar types of motion artifacts. In contrast, the textile device's fundamentally different design may confer advantages that are not fully reflected in this configuration, potentially leading to an underestimation of its performance. Therefore, this three-device comparison represents a conservative assessment of the textile electrodes. We estimate

TABLE IV: R-Peak detection performance of the two reference devices and the textile in lead II.

		BTL		
		detected	not det.	
Textile	detected	0.941 ± 0.062	0.004 ± 0.01	Faros
	not det.	0.002 ± 0.003	0.022 ± 0.037	
	detected	0.016 ± 0.026	0.007 ± 0.004	
	not det.	0.009 ± 0.011	-	

Dirichlet distributions for the observed events: hit, miss, and false alarm rates between pairs of devices with the results of the estimated distributions presented in Figure 8. Both estimates have a parameter configuration indicating that the majority of events are consistently identified by both devices. To compare the relevant distributions, we compute the log-likelihood ratio between $\mathcal{D}_{\text{Textile II}}^{\text{BTL II}}$ and $\mathcal{D}_{\text{Faros II}}^{\text{BTL II}}$, obtaining a value of 0.03 during the resting phase. This result suggests that both distributions provide similar likelihoods for the observed data. Additional results for other distributions and phases are provided in the supplementary material.

3) *Classification*: The AUC and F_1 scores are presented in Table V. For both tasks, the textile electrode achieve predictive performance that is similar to, or even surpasses, that of

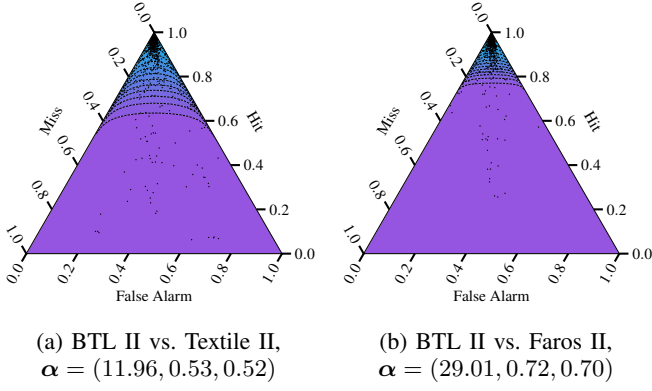


Fig. 8: Log density of the Dirichlet distribution and parameter vector α for miss, hit, and false alarm rates, using BTL lead II as reference and other leads for comparison.

machine learning models trained on features extracted from lead II of the reference system.

TABLE V: Machine Learning Results.

	Activity		Psychophysiological	
	AUC	F_1	AUC	F_1
BTL II	0.88 ± 0.03	0.72 ± 0.05	0.84 ± 0.05	0.68 ± 0.07
Textile II	0.88 ± 0.02	0.70 ± 0.04	0.91 ± 0.04	0.72 ± 0.05

4) *Morphological Assessment*: The extracted amplitude and interval values follow approximately a normal distribution. Outliers were removed prior to analysis. The Pearson correlation coefficient was computed between measurements from both devices for male and female subjects separately. Despite the significant spatial separation of electrode projections, we observe strong correlations between R-amplitudes, ST-amplitudes, and T-amplitudes, as well as between interval measures such as the QT interval, across different leads and study phases as presented in Table VI. Another finding is the pronounced influence of electrode positioning on amplitude values, particularly in the supine position. The P-wave amplitude exhibits a lower correlation, as it was more challenging to consistently detect the P-wave [81]. Additionally, substantial sex differences are evident, especially in the amplitude values of R-peaks for both lead I and lead II across all study phases indicate this impact. To further study the effect of this pronounced sex difference we rotate and scale the textile recordings as shown in Figure 9. The results of the alignment procedure, presented in Table VII, demonstrate improved cosine similarity S_c and reduced Frobenius distance after alignment, indicating enhanced correspondence between the recordings. The analysis of textile electrode placement as shown in Figure 3b and rotation angle reveals distinct sex-specific correlations. Among female participants, significant associations are observed between the rotation angle and the distances from both the upper (z1m) and lower (z2m) textile electrodes to the reference electrodes. Additionally, the distances from the upper reference electrode to the upper right (a2r) and upper left (a2l) textile electrodes also demonstrate

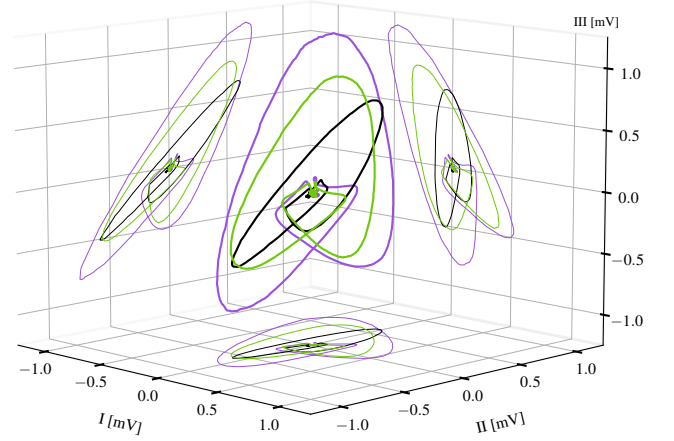


Fig. 9: 3D heart vector: BTL leads I/II/III (black), textile original (purple), and rotated/scaled (green) with 2D-plane projections.

significant correlations. Body height emerges as a notable influencing factor in females, whereas such correlations are considerably weaker in males. Conversely, in male participants, significant correlations with rotation are found for the distances to the upper reference electrodes, particularly z3l and a2l. Distances to the axillary line further contribute to the observed patterns in males. Collectively, these results highlight sex-specific differences in the factors affecting textile electrode placement and its relationship with biophysical measurements. In particular, for females, who generally have smaller body dimensions, the width and height of the upper body substantially impact ECG signal formation in textile electrode systems. This effect is especially important when electrodes are positioned closer to the body center, compared to the standard Einthoven placement.

IV. CONCLUSION

Our study presents a comprehensive assessment of ECG signal quality obtained from a wearable garment with textile-based dry electrodes, benchmarked against gold-standard Holter ECG systems. Our evaluation encompassed multiple dimensions, including SQIs, rhythm-based parameters, classification tasks relevant to physiological and psychophysiological states, and detailed morphological comparisons.

The results demonstrate that the textile-based system achieves concordance with reference devices in HR and HRV metrics across diverse activities and postures. Analysis of SQIs demonstrates that lead placement significantly influences signal quality. The textile system achieves signal quality comparable to medical grade reference devices, especially in the commonly used lead II. Machine learning-based classification tasks further confirms that features extracted from the textile system enable robust activity and task load discrimination, matching the performance of features from reference system recordings. Morphological analyses underline strong correlations between key ECG parameters recorded by textile and reference systems, although spatial and anatomical variations in electrode placement can affect amplitude values, most

TABLE VI: Pearson correlation r of morphological features extracted from reference and system under test with 95%CI indicated as $\pm r \left[\begin{smallmatrix} CI_{upper} \\ CI_{lower} \end{smallmatrix} \right]$ and $\text{abs}(r) > 0.3$ being in bold letters.

			R-Ampl.	QT-Int.	ST-Ampl.	T-Ampl.	T-Length	P-Ampl.
Female	Sitting	BTL/Textile I	+0.65 $\left[\begin{smallmatrix} +0.66 \\ +0.63 \end{smallmatrix} \right]$	+0.37 $\left[\begin{smallmatrix} +0.40 \\ +0.34 \end{smallmatrix} \right]$	+0.53 $\left[\begin{smallmatrix} +0.55 \\ +0.51 \end{smallmatrix} \right]$	+0.37 $\left[\begin{smallmatrix} +0.40 \\ +0.34 \end{smallmatrix} \right]$	+0.18 $\left[\begin{smallmatrix} +0.22 \\ +0.15 \end{smallmatrix} \right]$	+0.18 $\left[\begin{smallmatrix} +0.21 \\ +0.15 \end{smallmatrix} \right]$
		BTL/Textile II	+0.62 $\left[\begin{smallmatrix} +0.63 \\ +0.60 \end{smallmatrix} \right]$	+0.46 $\left[\begin{smallmatrix} +0.49 \\ +0.43 \end{smallmatrix} \right]$	+0.51 $\left[\begin{smallmatrix} +0.54 \\ +0.49 \end{smallmatrix} \right]$	+0.57 $\left[\begin{smallmatrix} +0.59 \\ +0.55 \end{smallmatrix} \right]$	+0.28 $\left[\begin{smallmatrix} +0.31 \\ +0.24 \end{smallmatrix} \right]$	+0.47 $\left[\begin{smallmatrix} +0.50 \\ +0.45 \end{smallmatrix} \right]$
	Lying	BTL/Textile I	+0.42 $\left[\begin{smallmatrix} +0.45 \\ +0.40 \end{smallmatrix} \right]$	+0.59 $\left[\begin{smallmatrix} +0.61 \\ +0.56 \end{smallmatrix} \right]$	+0.63 $\left[\begin{smallmatrix} +0.65 \\ +0.61 \end{smallmatrix} \right]$	+0.28 $\left[\begin{smallmatrix} +0.31 \\ +0.26 \end{smallmatrix} \right]$	+0.24 $\left[\begin{smallmatrix} +0.27 \\ +0.21 \end{smallmatrix} \right]$	+0.16 $\left[\begin{smallmatrix} +0.19 \\ +0.13 \end{smallmatrix} \right]$
		BTL/Textile II	+0.32 $\left[\begin{smallmatrix} +0.35 \\ +0.29 \end{smallmatrix} \right]$	+0.76 $\left[\begin{smallmatrix} +0.77 \\ +0.75 \end{smallmatrix} \right]$	+0.42 $\left[\begin{smallmatrix} +0.44 \\ +0.40 \end{smallmatrix} \right]$	+0.45 $\left[\begin{smallmatrix} +0.47 \\ +0.43 \end{smallmatrix} \right]$	+0.55 $\left[\begin{smallmatrix} +0.58 \\ +0.53 \end{smallmatrix} \right]$	+0.37 $\left[\begin{smallmatrix} +0.39 \\ +0.34 \end{smallmatrix} \right]$
	Moving	BTL/Textile I	+0.68 $\left[\begin{smallmatrix} +0.69 \\ +0.66 \end{smallmatrix} \right]$	+0.43 $\left[\begin{smallmatrix} +0.46 \\ +0.41 \end{smallmatrix} \right]$	+0.42 $\left[\begin{smallmatrix} +0.44 \\ +0.39 \end{smallmatrix} \right]$	+0.17 $\left[\begin{smallmatrix} +0.20 \\ +0.14 \end{smallmatrix} \right]$	+0.28 $\left[\begin{smallmatrix} +0.31 \\ +0.25 \end{smallmatrix} \right]$	+0.10 $\left[\begin{smallmatrix} +0.13 \\ +0.07 \end{smallmatrix} \right]$
		BTL/Textile II	+0.48 $\left[\begin{smallmatrix} +0.50 \\ +0.45 \end{smallmatrix} \right]$	+0.36 $\left[\begin{smallmatrix} +0.39 \\ +0.33 \end{smallmatrix} \right]$	+0.50 $\left[\begin{smallmatrix} +0.52 \\ +0.47 \end{smallmatrix} \right]$	+0.28 $\left[\begin{smallmatrix} +0.31 \\ +0.25 \end{smallmatrix} \right]$	+0.23 $\left[\begin{smallmatrix} +0.26 \\ +0.20 \end{smallmatrix} \right]$	+0.19 $\left[\begin{smallmatrix} +0.22 \\ +0.16 \end{smallmatrix} \right]$
Male	Sitting	BTL/Textile I	+0.80 $\left[\begin{smallmatrix} +0.81 \\ +0.79 \end{smallmatrix} \right]$	+0.45 $\left[\begin{smallmatrix} +0.47 \\ +0.43 \end{smallmatrix} \right]$	+0.67 $\left[\begin{smallmatrix} +0.69 \\ +0.66 \end{smallmatrix} \right]$	+0.40 $\left[\begin{smallmatrix} +0.42 \\ +0.38 \end{smallmatrix} \right]$	+0.21 $\left[\begin{smallmatrix} +0.23 \\ +0.18 \end{smallmatrix} \right]$	+0.31 $\left[\begin{smallmatrix} +0.34 \\ +0.29 \end{smallmatrix} \right]$
		BTL/Textile II	+0.18 $\left[\begin{smallmatrix} +0.21 \\ +0.16 \end{smallmatrix} \right]$	+0.36 $\left[\begin{smallmatrix} +0.38 \\ +0.34 \end{smallmatrix} \right]$	+0.59 $\left[\begin{smallmatrix} +0.61 \\ +0.57 \end{smallmatrix} \right]$	+0.43 $\left[\begin{smallmatrix} +0.45 \\ +0.41 \end{smallmatrix} \right]$	+0.08 $\left[\begin{smallmatrix} +0.10 \\ +0.05 \end{smallmatrix} \right]$	+0.13 $\left[\begin{smallmatrix} +0.16 \\ +0.10 \end{smallmatrix} \right]$
	Lying	BTL/Textile I	+0.75 $\left[\begin{smallmatrix} +0.76 \\ +0.74 \end{smallmatrix} \right]$	+0.36 $\left[\begin{smallmatrix} +0.38 \\ +0.34 \end{smallmatrix} \right]$	+0.41 $\left[\begin{smallmatrix} +0.43 \\ +0.39 \end{smallmatrix} \right]$	+0.38 $\left[\begin{smallmatrix} +0.40 \\ +0.36 \end{smallmatrix} \right]$	+0.09 $\left[\begin{smallmatrix} +0.12 \\ +0.07 \end{smallmatrix} \right]$	+0.38 $\left[\begin{smallmatrix} +0.40 \\ +0.36 \end{smallmatrix} \right]$
		BTL/Textile II	-0.39 $\left[\begin{smallmatrix} -0.37 \\ -0.41 \end{smallmatrix} \right]$	+0.57 $\left[\begin{smallmatrix} +0.58 \\ +0.55 \end{smallmatrix} \right]$	+0.35 $\left[\begin{smallmatrix} +0.37 \\ +0.32 \end{smallmatrix} \right]$	+0.26 $\left[\begin{smallmatrix} +0.28 \\ +0.24 \end{smallmatrix} \right]$	+0.11 $\left[\begin{smallmatrix} +0.13 \\ +0.08 \end{smallmatrix} \right]$	+0.02 $\left[\begin{smallmatrix} +0.04 \\ -0.01 \end{smallmatrix} \right]$
	Moving	BTL/Textile I	+0.75 $\left[\begin{smallmatrix} +0.76 \\ +0.74 \end{smallmatrix} \right]$	+0.24 $\left[\begin{smallmatrix} +0.26 \\ +0.22 \end{smallmatrix} \right]$	+0.44 $\left[\begin{smallmatrix} +0.46 \\ +0.42 \end{smallmatrix} \right]$	+0.14 $\left[\begin{smallmatrix} +0.16 \\ +0.12 \end{smallmatrix} \right]$	+0.13 $\left[\begin{smallmatrix} +0.16 \\ +0.10 \end{smallmatrix} \right]$	+0.12 $\left[\begin{smallmatrix} +0.15 \\ +0.10 \end{smallmatrix} \right]$
		BTL/Textile II	-0.09 $\left[\begin{smallmatrix} -0.07 \\ -0.12 \end{smallmatrix} \right]$	+0.24 $\left[\begin{smallmatrix} +0.27 \\ +0.22 \end{smallmatrix} \right]$	+0.24 $\left[\begin{smallmatrix} +0.26 \\ +0.22 \end{smallmatrix} \right]$	+0.08 $\left[\begin{smallmatrix} +0.10 \\ +0.05 \end{smallmatrix} \right]$	+0.11 $\left[\begin{smallmatrix} +0.14 \\ +0.09 \end{smallmatrix} \right]$	+0.05 $\left[\begin{smallmatrix} +0.07 \\ +0.02 \end{smallmatrix} \right]$

TABLE VII: Quality of Procrustes Alignment.

	RMSD	S_C	$\ A\ _F^2$
Original Textile & BTL	0.14 \pm 0.05	0.76 \pm 0.08	64.15 \pm 40.7
Rotated Textile & BTL	0.06 \pm 0.02	0.78 \pm 0.07	11.39 \pm 9.01

TABLE VIII: Pearson correlation r of rotation angles and anthropometric measurements with 95% CI.

	Female Rotation I/II	Male Rotation I/II
z1r	-0.26 $\left[\begin{smallmatrix} +0.02 \\ -0.47 \end{smallmatrix} \right]$	-0.09 $\left[\begin{smallmatrix} +0.18 \\ -0.33 \end{smallmatrix} \right]$
z2r	-0.16 $\left[\begin{smallmatrix} +0.11 \\ -0.39 \end{smallmatrix} \right]$	-0.09 $\left[\begin{smallmatrix} +0.18 \\ -0.33 \end{smallmatrix} \right]$
z1l	-0.24 $\left[\begin{smallmatrix} +0.03 \\ -0.46 \end{smallmatrix} \right]$	-0.19 $\left[\begin{smallmatrix} +0.08 \\ -0.42 \end{smallmatrix} \right]$
z2l	+0.14 $\left[\begin{smallmatrix} +0.38 \\ -0.13 \end{smallmatrix} \right]$	-0.08 $\left[\begin{smallmatrix} +0.18 \\ -0.33 \end{smallmatrix} \right]$
z1m	-0.56 $\left[\begin{smallmatrix} -0.32 \\ -0.70 \end{smallmatrix} \right]$	+0.23 $\left[\begin{smallmatrix} +0.44 \\ -0.05 \end{smallmatrix} \right]$
z2m	-0.45 $\left[\begin{smallmatrix} -0.18 \\ -0.61 \end{smallmatrix} \right]$	-0.14 $\left[\begin{smallmatrix} +0.13 \\ -0.38 \end{smallmatrix} \right]$
z3r	-0.32 $\left[\begin{smallmatrix} -0.04 \\ -0.51 \end{smallmatrix} \right]$	-0.21 $\left[\begin{smallmatrix} +0.07 \\ -0.43 \end{smallmatrix} \right]$
z3l	-0.24 $\left[\begin{smallmatrix} +0.04 \\ -0.45 \end{smallmatrix} \right]$	-0.42 $\left[\begin{smallmatrix} -0.15 \\ -0.60 \end{smallmatrix} \right]$
a1r	-0.29 $\left[\begin{smallmatrix} -0.02 \\ -0.50 \end{smallmatrix} \right]$	-0.12 $\left[\begin{smallmatrix} +0.15 \\ -0.36 \end{smallmatrix} \right]$
a2r	-0.41 $\left[\begin{smallmatrix} -0.14 \\ -0.59 \end{smallmatrix} \right]$	-0.01 $\left[\begin{smallmatrix} +0.25 \\ -0.26 \end{smallmatrix} \right]$
a1l	-0.22 $\left[\begin{smallmatrix} +0.06 \\ -0.44 \end{smallmatrix} \right]$	-0.12 $\left[\begin{smallmatrix} +0.15 \\ -0.35 \end{smallmatrix} \right]$
a2l	-0.46 $\left[\begin{smallmatrix} -0.20 \\ -0.69 \end{smallmatrix} \right]$	+0.44 $\left[\begin{smallmatrix} +0.61 \\ +0.18 \end{smallmatrix} \right]$
Height	+0.39 $\left[\begin{smallmatrix} +0.57 \\ +0.12 \end{smallmatrix} \right]$	-0.08 $\left[\begin{smallmatrix} +0.18 \\ -0.33 \end{smallmatrix} \right]$
Weight	-0.14 $\left[\begin{smallmatrix} +0.13 \\ -0.38 \end{smallmatrix} \right]$	-0.20 $\left[\begin{smallmatrix} +0.07 \\ -0.43 \end{smallmatrix} \right]$

notably in the supine position and among female participants. Our Procrustes alignment approach, incorporating rotation, enhances the morphological correspondence between systems and enables a more nuanced interpretation of inter-device differences. Notably, the investigation of electrode placement and anthropometric correlations revealed sex-specific determinants: especially for females, the distances between upper and lower textile electrodes and height are principal factors affecting rotation.

These findings collectively underscore the viability of textile electrode garments for long-term, ambulatory ECG monitoring, offering signal quality and diagnostic utility comparable to clinical gold standards. Importantly, the study highlights the necessity to account for sex-specific anatomical differences in

garment design and electrode placement to ensure equitable signal quality and diagnostic accuracy.

This work advances the evaluation of novel wearable textile ECG acquisition devices by introducing a rigorous, multi-faceted assessment framework. It comprehensively examines signal quality, usability in real-world applications, and incorporates sex-specific anatomical differences as well as key ergonomic and physiological determinants that inform the development of next-generation wearable ECG systems.

A. Limitations

Despite the robust design and comprehensive evaluation framework employed in this study, several limitations should be acknowledged. The electrode placement on the textile garment, although intended to closely approximate standardized locations, is inherently affected by anatomical variability and differences in garment fit among participants. These factors may influence signal quality and comparability with the reference systems. Although the cohort was balanced by sex and included a range of body types, the sample size may still limit the generalizability of findings, particularly regarding specific subpopulations or individuals with pathological cardiac conditions. Furthermore, all measurements were conducted under controlled laboratory conditions and predominantly involved healthy subjects; thus, performance under real-world ambulatory settings or in patient populations remains to be validated. Additionally, while objective SQIs and automated analysis were prioritized to minimize subjective bias, the lack of expert manual annotation may have led to an underestimation of device-specific artifacts or subtle diagnostic discrepancies. Finally, the scope of morphological comparisons is constrained by non-standardized lead projections, complicating direct equivalence between textile and clinical reference recordings. Future studies should address these limitations by incorporating larger and more diverse cohorts, testing in varied ambulatory environments, and including expert-annotated data for comprehensive clinical validation.

REFERENCES

- [1] W. Einthoven, "Die galvanometrische Registrierung des menschlichen Elektrokardiogramms, zugleich eine Beurtheilung der Anwendung des Capillar-Elektrometers in der Physiologie," *Physiologie des Menschen und der Tiere*, vol. 99, no. 9-10, Nov. 1903.
- [2] P. Kligfield, L. S. Gettes, J. J. Bailey, R. Childers, B. J. Deal, E. W. Hancock, G. van Herpen, J. A. Kors, P. Macfarlane, D. M. Mirvis, O. Pahlm, P. Rautaharju, and G. S. Wagner, "Recommendations for the Standardization and Interpretation of the Electrocardiogram: Part I: The Electrocardiogram and Its Technology: A Scientific Statement From the American Heart Association Electrocardiography and Arrhythmias Committee, Council on Clinical Cardiology; the American College of Cardiology Foundation; and the Heart Rhythm Society Endorsed by the International Society for Computerized Electrocardiology," *Circulation*, vol. 115, no. 10, Mar. 2007.
- [3] A. T. Reisner, G. D. Clifford, and R. G. Mark, "The Physiological Basis of the Electrocardiogram," in *Advanced Methods and Tools for ECG Data Analysis*, ser. Engineering in Medicine & Biology. Boston, London: Artech House, 2006.
- [4] J. W. Mason, E. W. Hancock, and L. S. Gettes, "Recommendations for the Standardization and Interpretation of the Electrocardiogram: Part II: Electrocardiography Diagnostic Statement List: A Scientific Statement From the American Heart Association Electrocardiography and Arrhythmias Committee, Council on Clinical Cardiology; the American College of Cardiology Foundation; and the Heart Rhythm Society: Endorsed by the International Society for Computerized Electrocardiology," *Circulation*, vol. 115, no. 10, Mar. 2007.
- [5] S. Stern, D. Tzivoni, and Z. Stern, "Diagnostic accuracy of ambulatory ECG monitoring in ischemic heart disease," *Circulation*, vol. 52, no. 6, Dec. 1975.
- [6] J. H. Eichhorn, "Standards for Patient Monitoring During Anesthesia at Harvard Medical School," *JAMA: The Journal of the American Medical Association*, vol. 256, no. 8, Aug. 1986.
- [7] M. Malik and A. J. Camm, "Evaluation of Drug-Induced QT Interval Prolongation: Implications for Drug Approval and Labelling," *Drug Safety*, vol. 24, no. 5, 2001.
- [8] V. Demmel, A. Sandberg-Schaal, J. B. Jacobsen, G. Golor, J. Pettersson, and A. Flint, "No QTc Prolongation with Semaglutide: A Thorough QT Study in Healthy Subjects," *Diabetes Therapy*, vol. 9, no. 4, Aug. 2018.
- [9] M. P. Oppelt, A. Foltyn, J. Deuschel, N. R. Lang, N. Holzer, B. M. Eskofier, and S. H. Yang, "ADABase: A Multimodal Dataset for Cognitive Load Estimation," *Sensors*, vol. 23, no. 1, p. 340, Dec. 2022.
- [10] B. Saha, L. Becker, J.-U. Garbas, M. Oppelt, A. Foltyn, S. Hettenkofer, N. Lang, M. Struck, N. Rohleder, and B. Mahesh, "Investigation of Relation between Physiological Responses and Personality during Stress Recovery," in *2021 IEEE International Conference on Pervasive Computing and Communications Workshops and Other Affiliated Events (PerCom Workshops)*. Kassel, Germany: IEEE, Mar. 2021.
- [11] K. Hansel, M. Tramontana, L. Bianchi, E. Cerulli, C. Patruno, M. Napolitano, and L. Stingeni, "Contact sensitivity to electrocardiogram electrodes due to acrylic acid: A rare cause of medical device allergy," *Contact Dermatitis*, vol. 82, no. 2, Feb. 2020.
- [12] C. Foti, A. Lopalco, L. Stingeni, K. Hansel, A. Lopodota, N. Denora, and P. Romita, "Contact allergy to electrocardiogram electrodes caused by acrylic acid without sensitivity to methacrylates and ethyl cyanoacrylate," *Contact Dermatitis*, vol. 79, no. 2, Jul. 2018.
- [13] J. Crawford and L. Doherty, *Practical Aspects of ECG Recording*. Cumbria [England]: M & K Update, 2012.
- [14] K. R. Evenson and C. L. Spade, "Review of Validity and Reliability of Garmin Activity Trackers," *Journal for the Measurement of Physical Behaviour*, vol. 3, no. 2, Jun. 2020.
- [15] R. Cao, I. Azimi, F. Sarhaddi, H. Niela-Vilen, A. Axelin, P. Liljeberg, and A. M. Rahmani, "Accuracy Assessment of Oura Ring Nocturnal Heart Rate and Heart Rate Variability in Comparison With Electrocardiography in Time and Frequency Domains: Comprehensive Analysis," *Journal of Medical Internet Research*, vol. 24, no. 1, Jan. 2022.
- [16] F. El-Amrawy and M. I. Nounou, "Are Currently Available Wearable Devices for Activity Tracking and Heart Rate Monitoring Accurate, Precise, and Medically Beneficial?" *Healthcare Informatics Research*, vol. 21, no. 4, 2015.
- [17] J. M. Peake, G. Kerr, and J. P. Sullivan, "A Critical Review of Consumer Wearables, Mobile Applications, and Equipment for Providing Biofeedback, Monitoring Stress, and Sleep in Physically Active Populations," *Frontiers in Physiology*, vol. 9, Jun. 2018.
- [18] J. Fine, K. L. Branan, A. J. Rodriguez, T. Boonya-ananta, Ajmal, J. C. Ramella-Roman, M. J. McShane, and G. L. Coté, "Sources of Inaccuracy in Photoplethysmography for Continuous Cardiovascular Monitoring," *Biosensors*, vol. 11, no. 4, p. 126, Apr. 2021.
- [19] D. S. Anceesh S. and J. Kozen Shih, "FDA Electrocardiograph Software for Over-The-Counter Use Regulatory Class: Class II," 2020.
- [20] W. Haverkamp, O. Göing, M. Anker, and S. D. Anker, "Vorhofflimmern-diagnostik mittels EKG-fähiger Smartwatches," *Der Nervenarzt*, vol. 93, no. 2, Feb. 2022.
- [21] C. Veltmann, J. R. Ehrlich, U. M. Gassner, B. Meder, M. Möckel, P. Radke, E. Scholz, H. Schneider, C. Stellbrink, and D. Duncker, "Wearable-basierte Detektion von Arrhythmien," *Der Kardiologe*, vol. 15, no. 4, pp. 341–353, Aug. 2021.
- [22] B. Bhargava, "AliveCor," *Journal of the Practice of Cardiovascular Sciences*, vol. 4, no. 1, 2018.
- [23] J. P. Halcox, K. Wareham, A. Cardew, M. Gilmore, J. P. Barry, C. Phillips, and M. B. Gravenor, "Assessment of Remote Heart Rhythm Sampling Using the AliveCor Heart Monitor to Screen for Atrial Fibrillation: The REHEARSE-AF Study," *Circulation*, vol. 136, no. 19, Nov. 2017.
- [24] E. H. Chung and K. D. Guise, "QTC intervals can be assessed with the AliveCor heart monitor in patients on dofetilide for atrial fibrillation," *Journal of Electrocardiology*, vol. 48, no. 1, Jan. 2015.
- [25] A. B. Nigusse, D. A. Mengistie, B. Malengier, G. B. Tsegahai, and L. V. Langenhove, "Wearable Smart Textiles for Long-Term Electrocardiography Monitoring- A Review," *Sensors*, vol. 21, no. 12, p. 4174, Jun. 2021.
- [26] M. Alizadeh-Meghbrazi, B. Ying, A. Schlums, E. Lam, L. Eskandarian, F. Abbas, G. Sidhu, A. Mahnam, B. Moineau, and M. R. Popovic, "Evaluation of dry textile electrodes for long-term electrocardiographic monitoring," *BioMedical Engineering OnLine*, vol. 20, no. 1, Jul. 2021.
- [27] L. Eskandarian, E. Lam, C. Rupnow, M. A. Meghbrazi, and H. E. Naguib, "Robust and Multifunctional Conductive Yarns for Biomedical Textile Computing," *ACS Applied Electronic Materials*, vol. 2, no. 6, pp. 1554–1566, Jun. 2020.
- [28] G. Acar, O. Ozturk, A. J. Golparvar, T. A. Elboshra, K. Böhringer, and M. K. Yapici, "Wearable and Flexible Textile Electrodes for Biopotential Signal Monitoring: A review," *Electronics*, vol. 8, no. 5, p. 479, Apr. 2019.
- [29] M. Catrysse, R. Puers, C. Hertleer, L. Van Langenhove, H. Van Egmond, and D. Matthys, "Towards the integration of textile sensors in a wireless monitoring suit," *Sensors and Actuators A: Physical*, vol. 114, no. 2-3, pp. 302–311, Sep. 2004.
- [30] J. C. Márquez, F. Seoane, E. Välimäki, and K. Lindecrantz, "Comparison of dry-textile electrodes for electrical bioimpedance spectroscopy measurements," *Journal of Physics: Conference Series*, vol. 224, p. 012140, Apr. 2010.
- [31] J. Yoo, Long Yan, Seulki Lee, Hyejung Kim, and Hoi-Jun Yoo, "A Wearable ECG Acquisition System With Compact Planar-Fashionable Circuit Board-Based Shirt," *IEEE Transactions on Information Technology in Biomedicine*, vol. 13, no. 6, Nov. 2009.
- [32] G. B. Tsegahai, B. Malengier, K. A. Fante, A. B. Nigusse, and L. Van Langenhove, "Integration of Conductive Materials with Textile Structures, an Overview," *Sensors*, vol. 20, no. 23, p. 6910, Dec. 2020.
- [33] D. Pani, A. Achilli, and A. Bonfiglio, "Survey on Textile Electrode Technologies for Electrocardiographic (ECG) Monitoring, from Metal Wires to Polymers," *Advanced Materials Technologies*, vol. 3, no. 10, pp. 1 800 008 (1–14), Oct. 2018.
- [34] D. Pani, A. Dessi, J. F. Saenz-Cogollo, G. Barabino, B. Fraboni, and A. Bonfiglio, "Fully Textile, PEDOT:PSS Based Electrodes for Wearable ECG Monitoring Systems," *IEEE Transactions on Biomedical Engineering*, vol. 63, no. 3, Mar. 2016.
- [35] A. A. Chalhawi, B. B. Narakathu, S. Emamian, B. J. Bazuin, and M. Z. Atashbar, "Development of printed and flexible dry ECG electrodes," *Sensing and Bio-Sensing Research*, vol. 20, pp. 9–15, Sep. 2018.
- [36] Y. T. Tsukada, M. Tokita, H. Murata, Y. Hirasawa, K. Yodogawa, Y.-K. Iwasaki, K. Asai, W. Shimizu, N. Kasai, H. Nakashima, and S. Tsukada, "Validation of wearable textile electrodes for ECG monitoring," *Heart and Vessels*, vol. 34, no. 7, Jul. 2019.
- [37] E. Lee and G. Cho, "PU nanoweb-based textile electrode treated with single-walled carbon nanotube/silver nanowire and its application to ECG monitoring," *Smart Materials and Structures*, vol. 28, no. 4, p. 045004, Apr. 2019.
- [38] N. T. Tasneem, S. A. Pullano, C. D. Critello, A. S. Fiorillo, and I. Mahbub, "A Low-Power On-Chip ECG Monitoring System Based on MWCNT/PMDS Dry Electrodes," *IEEE Sensors Journal*, vol. 20, no. 21, pp. 12 799–12 806, Nov. 2020.

- [39] G. Cho, K. Jeong, M. J. Paik, Y. Kwun, and M. Sung, "Performance Evaluation of Textile-Based Electrodes and Motion Sensors for Smart Clothing," *IEEE Sensors Journal*, vol. 11, no. 12, p. 3183, Dec. 2011.
- [40] M. Di Rienzo, V. Racca, F. Rizzo, B. Bordoni, G. Parati, P. Castiglioni, P. Meriggi, and M. Ferratini, "Evaluation of a textile-based wearable system for the electrocardiogram monitoring in cardiac patients," *EP Europace*, vol. 15, no. 4, Apr. 2013.
- [41] J. Lee, J. Heo, W. Lee, Y. Lim, Y. Kim, and K. Park, "Flexible Capacitive Electrodes for Minimizing Motion Artifacts in Ambulatory Electrocardiograms," *Sensors*, vol. 14, no. 8, Aug. 2014.
- [42] M. Weder, D. Hegemann, M. Amberg, M. Hess, L. Boesel, R. Abächerli, V. Meyer, and R. Rossi, "Embroidered Electrode with Silver/Titanium Coating for Long-Term ECG Monitoring," *Sensors*, vol. 15, no. 1, Jan. 2015.
- [43] A. Boehm, X. Yu, W. Neu, S. Leonhardt, and D. Teichmann, "A Novel 12-Lead ECG T-Shirt with Active Electrodes," *Electronics*, vol. 5, no. 4, p. 75, Nov. 2016.
- [44] X. Xiao, S. Pirbhulal, K. Dong, W. Wu, and X. Mei, "Performance Evaluation of Plain Weave and Honeycomb Weave Electrodes for Human ECG Monitoring," *Journal of Sensors*, vol. 2017, 2017.
- [45] F. Sun, C. Yi, W. Li, and Y. Li, "A wearable H-shirt for exercise ECG monitoring and individual lactate threshold computing," *Computers in Industry*, vol. 92–93, pp. 1–11, Nov. 2017.
- [46] X. An and G. Stylios, "A Hybrid Textile Electrode for Electrocardiogram (ECG) Measurement and Motion Tracking," *Materials*, vol. 11, no. 10, p. 1887, Oct. 2018.
- [47] A. Achilli, A. Bonfiglio, and D. Pani, "Design and Characterization of Screen-Printed Textile Electrodes for ECG Monitoring," *IEEE Sensors Journal*, vol. 18, no. 10, pp. 4097–4107, May 2018.
- [48] A. Ankhili, X. Tao, C. Cochrane, V. Koncar, D. Coulon, and J.-M. Tarlet, "Ambulatory Evaluation of ECG Signals Obtained Using Washable Textile-Based Electrodes Made with Chemically Modified PEDOT:PSS," *Sensors*, vol. 19, no. 2, p. 416, Jan. 2019.
- [49] L. Liu, X. Zhu, and Q. Xia, "An Integrated Design of Multi-Channel ECG Sensor on Smart Garment," in *Proceedings of the 2020 10th International Conference on Biomedical Engineering and Technology*. Tokyo Japan: ACM, Sep. 2020, pp. 316–320.
- [50] K. Arquilla, L. Devendorf, A. K. Webb, and A. P. Anderson, "Detection of the Complete ECG Waveform with Woven Textile Electrodes," *Biosensors*, vol. 11, no. 9, p. 331, Sep. 2021.
- [51] D. Bläsing, A. Buder, J. E. Reiser, M. Nisser, S. Derlien, and M. Vollmer, "ECG performance in simultaneous recordings of five wearable devices using a new morphological noise-to-signal index and Smith-Waterman-based RR interval comparisons," *PLOS ONE*, vol. 17, no. 10, Oct. 2022.
- [52] L. Neri, I. Corazza, M. T. Oberdier, J. Lago, I. Gallelli, A. F. Cicero, I. Diemberger, A. Orro, A. Beker, N. Paolucci, H. R. Halperin, and C. Borghi, "Comparison Between a Single-Lead ECG Garment Device and a Holter Monitor: A Signal Quality Assessment," *Journal of Medical Systems*, vol. 48, no. 1, p. 57, May 2024.
- [53] T. Pola and J. Vanhala, "Textile Electrodes in ECG Measurement," in *2007 3rd International Conference on Intelligent Sensors, Sensor Networks and Information*. Melbourne, Australia: IEEE, 2007.
- [54] H. Qin, J. Li, B. He, J. Sun, L. Li, and L. Qian, "Novel Wearable Electrodes Based on Conductive Chitosan Fabrics and Their Application in Smart Garments," *Materials*, vol. 11, no. 3, p. 370, Mar. 2018.
- [55] E. Gunnarsson, K. Rödbj, and F. Seoane, "Seamlessly integrated textile electrodes and conductive routing in a garment for electrostimulation: Design, manufacturing and evaluation," *Scientific Reports*, vol. 13, no. 1, Oct. 2023.
- [56] E. Bihar, T. Roberts, E. Ismailova, M. Saadaoui, M. Isik, A. Sanchez-Sanchez, D. Mecerreyes, T. Hervé, J. B. De Graaf, and G. G. Malliaras, "Fully Printed Electrodes on Stretchable Textiles for Long-Term Electrophysiology," *Advanced Materials Technologies*, vol. 2, no. 4, p. 1600251, Apr. 2017.
- [57] T. Takeshita, M. Yoshida, Y. Takei, A. Ouchi, A. Hinoki, H. Uchida, and T. Kobayashi, "Relationship between Contact Pressure and Motion Artifacts in ECG Measurement with Electrostatic Flocked Electrodes Fabricated on Textile," *Scientific Reports*, vol. 9, no. 1, Apr. 2019.
- [58] M. J. Yarnoz and A. B. Curtis, "More Reasons Why Men and Women Are Not the Same (Gender Differences in Electrophysiology and Arrhythmias)," *The American Journal of Cardiology*, vol. 101, no. 9, May 2008.
- [59] O. Kittnar, "Sex Related Differences in Electrocardiography," *Physiological Research*, Jul. 2023.
- [60] C. Prajapati, J. Koivumäki, M. Pekkanen-Mattila, and K. Aalto-Setälä, "Sex differences in heart: From basics to clinics," *European Journal of Medical Research*, vol. 27, no. 1, Nov. 2022.
- [61] P. M. Rautaharju, L. Park, F. S. Rautaharju, and R. Crow, "A standardized procedure for locating and documenting ecg chest electrode positions: Consideration of the effect of breast tissue on ecg amplitudes in women," *Journal of Electrocardiology*, vol. 31, no. 1, Jan. 1998.
- [62] R. Colaco, P. Reay, C. Beckett, T. C. Aitchison, and P. W. Macfarlane, "False positive ECG reports of anterior myocardial infarction in women," *Journal of Electrocardiology*, vol. 33, Jan. 2000.
- [63] B. J. Drew, "Pitfalls and Artifacts in Electrocardiography," *Cardiology Clinics*, vol. 24, no. 3, Aug. 2006.
- [64] "DIN EN ISO 8559-1:2021-04, Größenbezeichnung von Bekleidung - Teil 1: Anthropometrische Definition für Körpermaße (ISO_8559-1:2017); Deutsche Fassung EN_ISO_8559-1:2020."
- [65] S. M. Jaeggi, M. Buschkuehl, W. J. Perrig, and B. Meier, "The concurrent validity of the N-Back task as a working memory measure," *Memory*, vol. 18, no. 4, pp. 394–412, 2010.
- [66] G. D. Clifford, D. Lopez, Q. Li, and I. Rezek, "Signal quality indices and data fusion for determining acceptability of electrocardiograms collected in noisy ambulatory environments," in *Computing in Cardiology*, Hangzhou, China, 2011.
- [67] J. Behar, J. Oster, Q. Li, and G. D. Clifford, "A single channel ECG quality metric," in *Computing in Cardiology*, vol. 2012 Computing in Cardiology, Krakow, Poland, 2012, pp. 381–384.
- [68] Z. Zhao and Y. Zhang, "SQI Quality Evaluation Mechanism of Single-Lead ECG Signal Based on Simple Heuristic Fusion and Fuzzy Comprehensive Evaluation," *Frontiers in Physiology*, vol. 9, p. 727, Jun. 2018.
- [69] D. Hayn, B. Jammerbund, and G. Schreier, "QRS detection based ECG quality assessment," *Physiological Measurement*, vol. 33, no. 9, Sep. 2012.
- [70] G. B. Moody, "The XQRS algorithm." <https://wfdb.readthedocs.io/en/latest/processing.html>, Jun. 2022.
- [71] T. Rodrigues, S. Samoutphonh, H. Silva, and A. Fred, "A Low-Complexity R-peak Detection Algorithm with Adaptive Thresholding for Wearable Devices," in *2020 25th International Conference on Pattern Recognition (ICPR)*. Milan, Italy: IEEE, Jan. 2021, pp. 1–8.
- [72] F. Shaffer and J. P. Ginsberg, "An Overview of Heart Rate Variability Metrics and Norms," *Frontiers in Public Health*, vol. 5, p. 258, Sep. 2017.
- [73] G. D. Clifford, F. Azuaje, and P. McSharry, Eds., *Advanced Methods and Tools for ECG Data Analysis*. Boston: Artech House, 2006.
- [74] P. Hamilton, "Open source ECG analysis," in *Computers in Cardiology*. Memphis, TN, USA: IEEE, 2002, pp. 101–104.
- [75] T. P. Minka, "Estimating a Dirichlet distribution," 2012.
- [76] L. Yang, L. Gan, Z. Zhang, Z. Zhang, H. Yang, Y. Zhang, and J. Wu, "Insight into the Contact Impedance between the Electrode and the Skin Surface for Electrophysical Recordings," *ACS Omega*, vol. 7, no. 16, pp. 13 906–13 912, Apr. 2022.
- [77] K. Goyal, D. A. Borkholder, and S. W. Day, "Dependence of Skin-Electrode Contact Impedance on Material and Skin Hydration," *Sensors*, vol. 22, no. 21, p. 8510, Nov. 2022.
- [78] M. S. Toosi and M. T. Sochanski, "False ST elevation in a modified 12-lead surface electrocardiogram," *Journal of Electrocardiology*, vol. 41, no. 3, pp. 197–201, May 2008.
- [79] V. Salvi, D. R. Karnad, G. K. Panicker, M. Natekar, P. Hingorani, V. Kerkar, A. Ramasamy, M. De Vries, T. Zumbrennen, S. Kothari, and D. Narula, "Comparison of 5 methods of QT interval measurements on electrocardiograms from a thorough QT/QTc study: Effect on assay sensitivity and categorical outliers," *Journal of Electrocardiology*, vol. 44, no. 2, pp. 96–104, Mar. 2011.
- [80] L. Li, J. Camps, B. Rodriguez, and V. Grau, "Solving the Inverse Problem of Electrocardiography for Cardiac Digital Twins: A Survey," *IEEE Reviews in Biomedical Engineering*, vol. 18, pp. 316–336, 2025.
- [81] L. Maršánová, A. Nemcova, R. Smisek, L. Smital, and M. Vitek, "Brno University of Technology ECG Signal Database with Annotations of P Wave (BUT PDB)," 2021.

Supplementary Materials

I. SIGNAL PREPROCESSING

This work does not primarily focus on improving, filtering, or enhancing signal quality by the development of novel filtering techniques or fiducial point extraction algorithms. Instead, we rely on established state-of-the-art signal processing methods for Electrocardiography (ECG) signals.

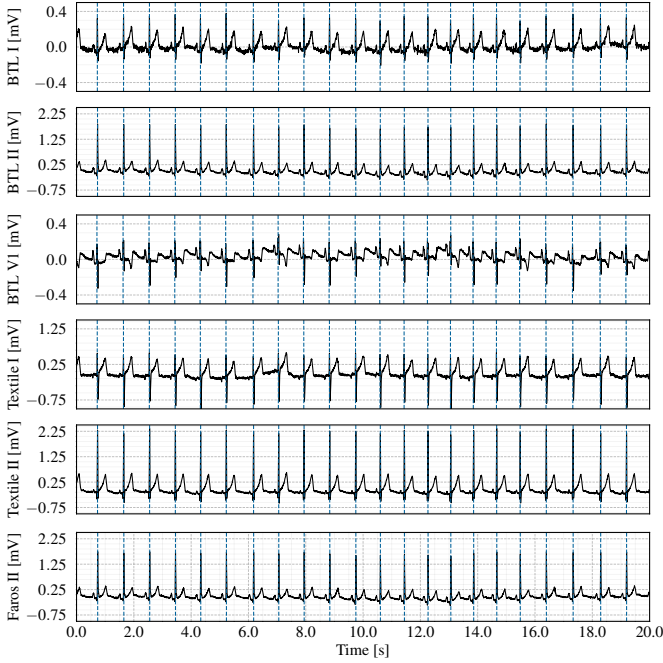


Fig. 1: Visualization of recorded channels and devices. The signal shows different signal amplitude values during a sitting phase with a resting heart rate and annotated peak locations.

A. Signal Quality and Filtering

Noise in ECG signals manifests on different time scales with characteristic spectral structures [1], [2]. Baseline wander artifacts are caused by changes in skin-electrode impedance e.g. by sweating and other types of slow drifts, that are caused by body movements or respiration. These artifacts are typically present in the spectral range between 0.01 and 1 Hz [3]. It is noteworthy that artifacts below a threshold of 0.67 Hz can be removed with linear digital zero-phase distortion filters according to the American National Standards Institute/Advancement of Medical Instrumentation (ANSI/AAMI) recommendations for standard clinical ECGs [4]. However, spectral components above this threshold or filters with a higher cutoff frequency can distort ST-segment related abnormalities. Another common artifact is caused by power line interference. This artifact manifests itself in a narrowband spectral component at 50 Hz or 60 Hz and its harmonics and is especially critical as it can

distort morphological signal properties such as the P-wave. These artifacts are commonly filtered with notch filters [3]. Artifacts caused by the electrical activity of skeletal muscles are prominently present in the spectral bandwidth between 20 Hz and 10 kHz and can therefore interfere with ECG signal information [1]. The research community has developed different methods to mitigate the effect of these artifacts, like removing them with adaptive filters or wavelet transformations [5], consider practical aspects like changing the electrode positions for certain activities, or utilizing end-to-end trained deep learning models [6], [7], that either denoise the ECG for further processing or learning embeddings that are not prone to noise.

We opted to only filter baseline noise using a forward and backward highpass filter with a cutoff frequency of 0.67 Hz and recorded the signals in our lab apart from potential 50Hz (the study was conducted in Germany) noise sources. The precaution of powerline noise filtering was not necessary in our setup, as the study was conducted away from power lines and no phases exhibited visible powerline noise. However, such noise could potentially be introduced during the *Walking* or *Running* activities on the treadmill.

II. SUPPLEMENTARY RESULTS

A. Signal Quality Indices

To complement the findings presented in the main article, we provide the Signal Quality Indices (SQIs) for female and male subjects separately in Sup. Figures 2 and 3, respectively. Across all systems—including the reference systems BTL and Faros, as well as the textile wearable garment—the general trend persists: lead II demonstrates superior performance for these signal quality metrics. Notably, within the male subgroup, the textile garment exhibits significantly lower morphology-based SQIs in both lead I and Lead II compared to the female subgroup. This observation warrants further investigation, as factors such as garment fit or body shape may contribute to the observed reduction in signal quality indices. Future studies should address these potential influences to better understand the underlying causes of this performance disparity.

B. R-Peak detection and Deliniation

R-peak detection in ECG signals is essential for accurate heart rate analysis and the diagnosis of cardiac abnormalities, as it identifies the QRS complex peaks associated with ventricular depolarization. The Pan-Tompkins algorithm remains a cornerstone in this field, employing a sequence of filtering, differentiation, and adaptive thresholding to achieve reliable real-time R-peak detection [8]. Building upon this foundation, advanced approaches such as wavelet transforms and machine learning techniques have been developed to further enhance

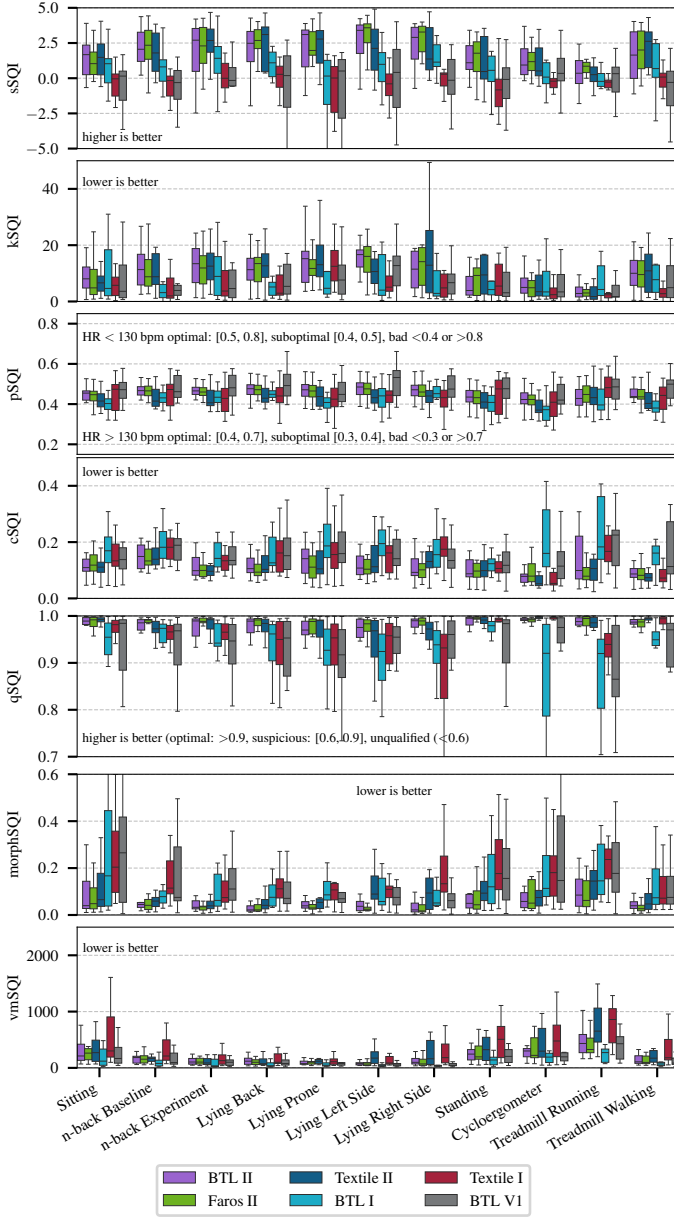


Fig. 2: SQIs for female subjects.

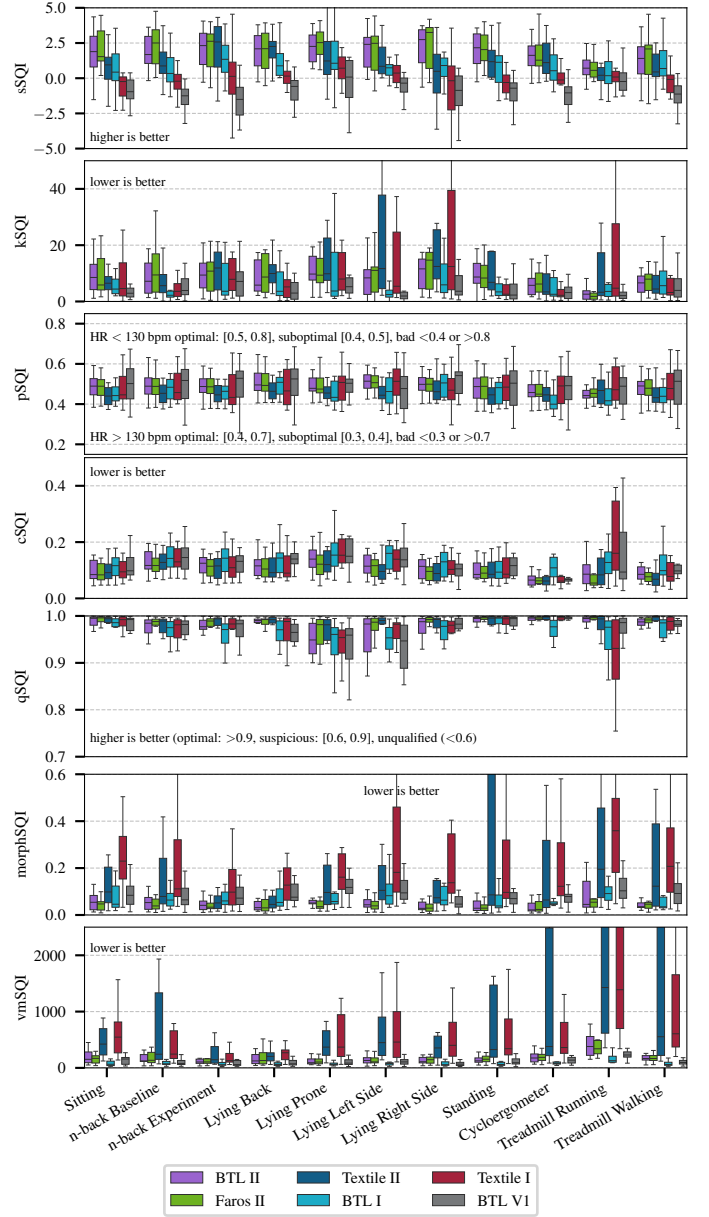


Fig. 3: SQIs for male subjects.

detection robustness in the presence of noise and signal variability. The widespread adoption and validation of these algorithms have been facilitated by benchmark datasets, most notably the MIT-BIH arrhythmia database [9], which continues to support progress and standardization in R-peak detection research. Nowadays, several publicly available software packages provide a variety of state-of-the-art R-peak detection algorithms, which often differ only in minor methodological improvements. Performance comparisons reveal that no single algorithm consistently outperforms others across all datasets; rather, the relative effectiveness of an algorithm can vary depending on the specific characteristics of the data.

To address potential biases arising from algorithm selection, we adopt the following strategies. First, for evaluating R-peak detection quality, we employ multiple algorithms specifically, the Hamilton [10], Pan-Tompkins [8], and Rodrigues [11]

methods and concatenate the detection results to mitigate the influence of any single algorithm's performance. Second, for our machine learning experiments, we utilize the Rodrigues algorithm that shows promising results over wearable devices [11]. Third, for ECG delineation (fiducial point detection), we follow the approach described in [12]. All algorithms are implemented in Python using the NeuroKit2 toolbox [13]. In this study, we did not evaluate the performance of the peak detection and delineation algorithms. Instead, we selected an algorithm previously employed for this specific application and deferred the optimization of detection algorithms to future work.

C. Computing the median complex

Throughout this paper, we employ the computation of a median complex, for example, when performing Procrustes

alignment between two ECG devices. We compute these median complexes by first extracting the R-peak locations and which in turn are then used to align the heart beats, as illustrated in gray in Sup. Fig. 4. The median complex is subsequently computed over all aligned complexes. These

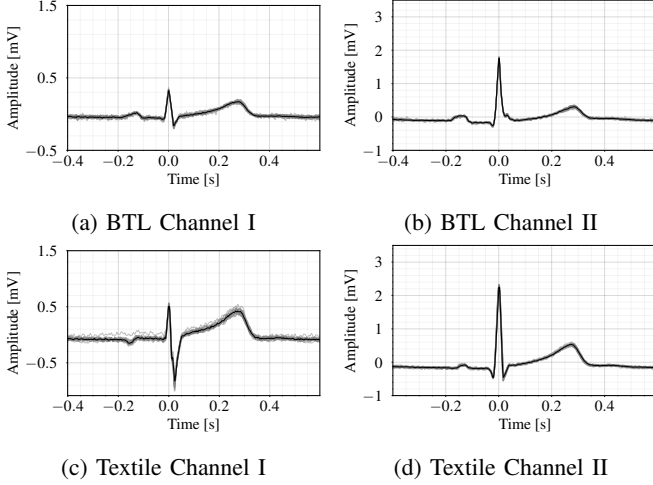


Fig. 4: Heart beats aligned on the R-peaks and computed median complex for a 30s window during rest of the same subject.

median complexes can then be shown in the I/II planes (see Sup. Fig. 5) and rotated such that they better align with each other.

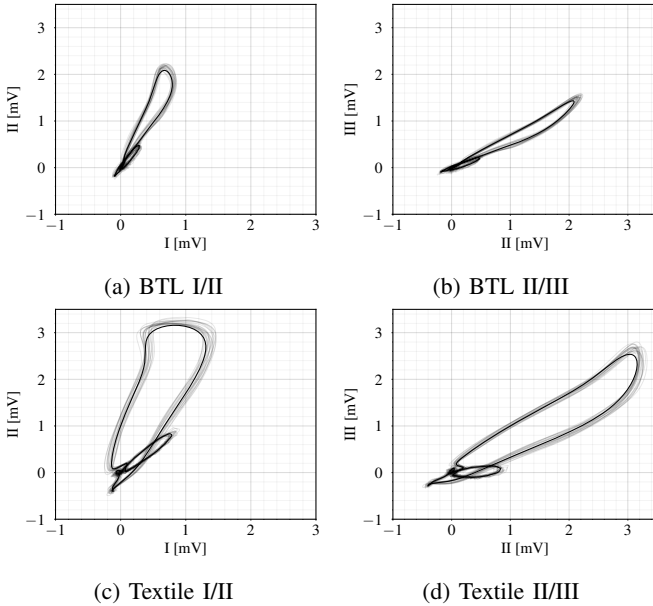


Fig. 5: Vector visualizations over complexes within a 30s window and median complex during rest of the same subject.

D. Recording data

The sampling frequency of the ECG devices employed in this study varied among the platforms utilized. Specifically, the BTL device operated at a sampling frequency of 500 Hz, the

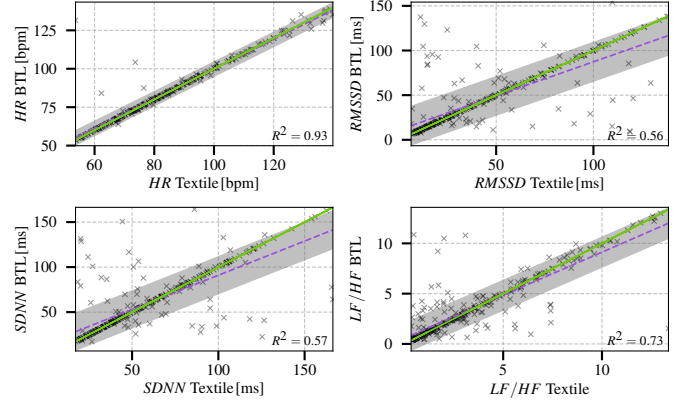


Fig. 6: Correlation of physiological parameters measured in Lead II of two devices, the reference system BTL on the y-axis and the textile on the x-axis. With optimal correlation (green) and actual fit (purple).

Faros device at 1000 Hz, and the textile device at 400 Hz. To ensure methodological consistency and facilitate subsequent data analyses, all ECG recordings were resampled to a uniform frequency of 1000 Hz. This standardization was chosen for simplicity, as computational constraints associated with higher sampling rates were not a limiting factor in the context of this post-hoc analysis.

E. Synchronization

The BTL device was consistently initiated first and terminated last during each recording session. Subsequently, either the Faros or the textile were started and stopped independently. To achieve temporal alignment among recordings, data from the Faros and textile were divided into 30s segments, which were then convolved with the raw BTL signal. Given the inherent irregularity of heart rate, these segments intersect with the BTL signal only at specific points, producing a pronounced maximum in the correlation function. The temporal shift corresponding to this maximum was used to synchronize the signals across devices. The accuracy of this alignment method was validated in several ways. A button on the BTL system was pressed after the initiation of the other devices and the start of the study protocol, enabling the extraction of an event marker for subsequent comparison. Additional confirmation was obtained through visual inspection and by referencing the onboard clocks of the devices. Notably, this approach eliminates the requirement for any physical electrical connections or wiring between devices. Furthermore, over the relatively short duration of our recordings, we did not observe any significant clock drift among the systems.

F. Peak Detection

To complement the findings presented in the main document, we provide the raw data of hit, miss, and false alarm rates in Sup. Table I and Sup. Table II, reporting both mean and standard deviation values. The results indicate a marked decline in the hit rates and an increase in miss and false alarm

rates for the BTL/textile system compared to the BTL/Faros device, particularly during the *Running* and *Lying* phases. In contrast, performance during the *Sitting* phase and less intensive upright activities, such as the *Cycloergometer* and *Walking* phases, remains comparable between the two systems.

A comparison of detection performance between female and male participants in our R-peak detection experiments revealed no significant differences. This finding aligns with our main article, suggesting that for tasks relying primarily on R-peak detection, such as the assessment of heart rhythm or heart rate variability, sex does not constitute a major influencing factor.

TABLE I: R-Peak detection performance between BTL lead II and textile lead II for both sexes.

		Hit	Miss	False Alarm
Female	Sitting Relaxed	0.97 ± 0.06	0.02 ± 0.03	0.02 ± 0.03
	Sitting Video	0.95 ± 0.08	0.02 ± 0.04	0.03 ± 0.06
	<i>n</i> -Back	0.96 ± 0.08	0.02 ± 0.04	0.02 ± 0.05
	Lying Back	0.95 ± 0.08	0.02 ± 0.04	0.03 ± 0.05
	Lying Left	0.93 ± 0.13	0.03 ± 0.05	0.04 ± 0.09
	Lying Right	0.93 ± 0.11	0.02 ± 0.04	0.05 ± 0.09
	Lying Stomach	0.94 ± 0.08	0.03 ± 0.05	0.03 ± 0.05
	Standing	0.96 ± 0.06	0.02 ± 0.05	0.01 ± 0.02
	Ergometer	0.98 ± 0.03	0.01 ± 0.02	0.01 ± 0.01
	Running	0.84 ± 0.26	0.09 ± 0.17	0.07 ± 0.10
	Walking	0.96 ± 0.09	0.02 ± 0.04	0.02 ± 0.05
Male	Sitting Relaxed	0.97 ± 0.05	0.02 ± 0.04	0.01 ± 0.02
	Sitting Video	0.95 ± 0.08	0.02 ± 0.04	0.03 ± 0.06
	<i>n</i> -Back	0.96 ± 0.08	0.02 ± 0.04	0.02 ± 0.06
	Lying Back	0.96 ± 0.07	0.02 ± 0.05	0.02 ± 0.04
	Lying Left	0.93 ± 0.13	0.04 ± 0.07	0.03 ± 0.07
	Lying Right	0.89 ± 0.24	0.05 ± 0.09	0.07 ± 0.17
	Lying Stomach	0.88 ± 0.18	0.06 ± 0.08	0.07 ± 0.13
	Standing	0.96 ± 0.07	0.02 ± 0.05	0.01 ± 0.03
	Ergometer	0.94 ± 0.15	0.04 ± 0.10	0.02 ± 0.05
	Running	0.91 ± 0.14	0.04 ± 0.07	0.05 ± 0.07
	Walking	0.93 ± 0.15	0.03 ± 0.05	0.04 ± 0.12

As supplementary comparison between our male and female population Table III and Table IV are presented in accordance to our main article.

G. Alignment

ECGs acquired using different measurement systems, differing in aspects such as skin-electrode contact quality, electrode placement, or lead orientation, may exhibit signal variability, even though both capture the same underlying cardiac electrical activity. This variability can be attributed to factors including tissue composition at the measurement sites, proximity of the electrodes to the heart, and the electrical properties of the skin-to-electrode interface. We therefore can only approximate the transformation between the two recordings as

TABLE II: R-Peak detection performance between BTL Lead II and Faros Lead II for both sexes.

		Hit	Miss	False Alarm
Female	Sitting Relaxed	0.96 ± 0.06	0.02 ± 0.03	0.02 ± 0.04
	Sitting Video	0.96 ± 0.06	0.02 ± 0.04	0.02 ± 0.03
	<i>n</i> -Back	0.96 ± 0.07	0.02 ± 0.05	0.01 ± 0.03
	Lying Back	0.96 ± 0.06	0.02 ± 0.04	0.02 ± 0.02
	Lying Left	0.95 ± 0.07	0.03 ± 0.05	0.02 ± 0.03
	Lying Right	0.97 ± 0.04	0.01 ± 0.02	0.01 ± 0.02
	Lying Stomach	0.95 ± 0.07	0.02 ± 0.04	0.03 ± 0.06
	Standing	0.98 ± 0.03	0.01 ± 0.02	0.01 ± 0.01
	Ergometer	0.97 ± 0.03	0.01 ± 0.02	0.01 ± 0.02
	Running	0.91 ± 0.17	0.04 ± 0.09	0.05 ± 0.09
	Walking	0.97 ± 0.05	0.02 ± 0.03	0.02 ± 0.03
Male	Sitting Relaxed	0.98 ± 0.04	0.01 ± 0.02	0.01 ± 0.02
	Sitting Video	0.96 ± 0.07	0.02 ± 0.04	0.02 ± 0.03
	<i>n</i> -Back	0.96 ± 0.10	0.02 ± 0.05	0.02 ± 0.06
	Lying Back	0.97 ± 0.06	0.02 ± 0.04	0.02 ± 0.04
	Lying Left	0.95 ± 0.10	0.02 ± 0.06	0.02 ± 0.06
	Lying Right	0.96 ± 0.11	0.03 ± 0.06	0.02 ± 0.05
	Lying Stomach	0.93 ± 0.12	0.04 ± 0.07	0.03 ± 0.06
	Standing	0.98 ± 0.03	0.01 ± 0.01	0.01 ± 0.02
	Ergometer	0.99 ± 0.02	0.01 ± 0.01	0.01 ± 0.01
	Running	0.97 ± 0.04	0.01 ± 0.01	0.02 ± 0.02
	Walking	0.97 ± 0.04	0.02 ± 0.03	0.01 ± 0.02

TABLE III: Male R-Peak Detection Matrix

	BTL		
	detected	not det.	
Textile	detected	0.929 ± 0.078	0.002 ± 0.003
	not det.	0.001 ± 0.002	0.032 ± 0.049
	detected	0.024 ± 0.035	0.006 ± 0.003
	not det.	0.006 ± 0.003	-

TABLE IV: Female R-Peak Detection Matrix

	BTL		
	detected	not det.	
Textile	detected	0.953 ± 0.039	0.007 ± 0.014
	not det.	0.003 ± 0.003	0.012 ± 0.01
	detected	0.006 ± 0.005	0.008 ± 0.005
	not det.	0.012 ± 0.014	-

ECGs inherently resemble an inverse problem, as the signals recorded on the skin surface represent the aggregated activity of numerous cardiac cells, rather than direct measurements of the underlying sources of activation.

Despite these differences, we opted to approximate the

underlying signals for comparative analysis, by adopting a two-dimensional transformation on the leads I/II plane from one system to the other, with lead III being defined by lead III = lead II - lead I.

To align the recordings from the two systems, we employ a rotational Procrustes alignment, constraining the rotation matrix according to established mathematical properties: the transpose of the rotation matrix equals its inverse ($R^T = R^{-1}$), and the determinant of the matrix is unity ($|R| = 1$). Formally, given an ECG recording $\mathbf{A} \in \mathbb{R}^{m \times n}$ and a reference ECG $\mathbf{B} \in \mathbb{R}^{m \times n}$ where $n = 2$ represents the two approximated leads, and m denotes the number of samples within a single median complex.

We seek a rotation matrix $\mathbf{R} \in \mathbb{R}^{n \times n}$ that minimizes the Frobenius norm of the difference between the rotated recording and the reference. This optimization problem is described in Equation 1 in the main article. To further account for gain discrepancies in the recordings attributable to factors like electrode properties, we introduce a linear scaling such that the maximum magnitude in I/II of \mathbf{A} is the same as the maximum magnitude in lead I/II of \mathbf{B} .

Algorithm 1: Algorithm for median complex projection alignment of textile median complex \mathbf{A} and reference median complex \mathbf{B} using rotation matrix \mathbf{R} and scaling s .

Input: \mathbf{A}, \mathbf{B}

Output: \mathbf{R}, s

- 1: $|\mathbf{v}|_{\mathbf{A}} = \sqrt{I_A^2 + II_A^2}$
- 2: $|\mathbf{v}|_{\mathbf{B}} = \sqrt{I_B^2 + II_B^2}$
- 3: $s = \frac{\text{abs}(\max(|\mathbf{v}|_{\mathbf{A}}))}{\text{abs}(\max(|\mathbf{v}|_{\mathbf{B}}))}$
- 4: $\mathbf{A}' = s\mathbf{A}$
- 5: $\mathbf{R} \leftarrow \min(\|\mathbf{A}'\mathbf{R} - \mathbf{B}\|_F^2)$
- 6: **return** \mathbf{R}, s

As this approximation is to our knowledge not used in literature, we report the quality of the fit in the main paper using three different metrics: First, the squared Frobenius norm error of N samples and D dimension lead vector of the difference matrix is computed as

$$\|\mathbf{A} - \mathbf{B}\|_F^2 = \sum_{i=1}^N \sum_{j=1}^D (a_{ij} - b_{ij})^2 \quad (1)$$

providing a global measure of the aggregate deviation across all leads and time points. Second, the root-mean-square deviation (RMSD) is calculated to offer a normalized metric of average discrepancy, defined as

$$\text{RMSD} = \sqrt{\frac{1}{N} \sum_{i=1}^N \sum_{j=1}^D (a_{ij} - b_{ij})^2} \quad (2)$$

Lastly, we utilize the cosine similarity, S_C , to quantify the degree of alignment in signal directionality between the two recordings. For N -dimensional ECG signal vectors \mathbf{A} and \mathbf{B} , this is computed as

$$S_C = \frac{1}{N} \sum_{i=1}^N \frac{\sum_{j=1}^D a_{ij} b_{ij}}{\sqrt{\sum_{j=1}^D a_{ij}^2} \sqrt{\sum_{j=1}^D b_{ij}^2}} \quad (3)$$

We present lead I of the rotated and scaled textile recording



Fig. 7: BTL and Textile lead I and the projected version after rotating and scaling.

alongside the reference system in Sup. Fig. 7. The results indicate that, after the alignment procedure, the R-peak amplitude recorded by the textile system more closely corresponds to that of the BTL system. Additionally, the ratio of the R-peak to the T-wave in the aligned textile signal more closely resembles the ECG of the reference system than the unprocessed textile recording. Nevertheless, a notable limitation persists: the T-wave remains inverted in the textile recording compared to the reference system, showing that it is no trivial task to approximate one recording to another recording.

H. Estimating Dirichlet distributions

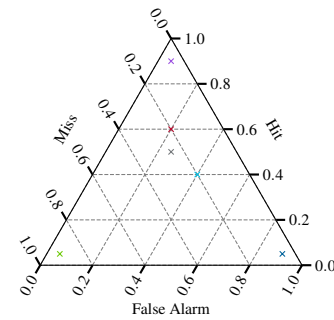


Fig. 8: Triangle plot to visualize variables using a ternary plot. All points within the triangle, in our sum of all hit, miss and false alarms sums up to 1. Purple: (Hit 0.9, Miss 0.05 and False Alarm 0.05), Green: (Hit 0.05, Miss 0.9 and False Alarm 0.05), Dark-Blue: (Hit 0.05, Miss 0.05 and False Alarm 0.9), Light-Blue: (Hit 0.4, Miss 0.2 and False Alarm 0.4), Red: (Hit 0.6, Miss 0.1 and False Alarm 0.2), Grey: (Hit 0.5, Miss 0.25 and False Alarm 0.25)

Hit Rate, Miss Rate and False Alarm Rate are mutually exclusive and sum up to one (It is either hit, miss or false alarm).

Using observations from multiple subjects and detectors, we are estimating a Dirichlet distribution given by Equation (4):

$$\mathcal{D}(\alpha) = \frac{1}{B(\alpha)} \prod_{i=1}^K x_i^{\alpha_i - 1} \quad (4)$$

where the beta function $B(\alpha)$ shown in Equation 5 express by gamma functions $\Gamma(\alpha)$

$$B(\alpha) = \frac{\prod_{i=1}^K \Gamma(\alpha_i)}{\Gamma(\alpha_0)} \quad (5)$$

and parameter α_0 given by Equation 6

$$\alpha_0 = \sum_{i=1}^K \alpha_i \quad (6)$$

using maximum likelihood estimations [14]. We report the parameter vector $\alpha = (\alpha_1, \alpha_2, \alpha_3)$ and the visualization of the estimated Dirichlet distribution in Sup. Fig. 9.

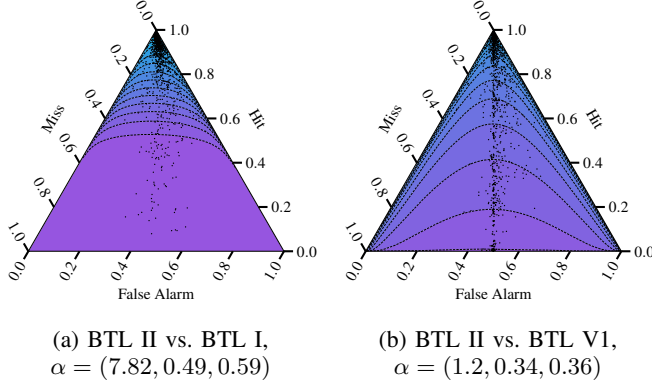


Fig. 9: Log density of the Dirichlet distribution visualization and α parameter vector of miss, hit and false alarm values with BTL lead II as reference and BTL leads I and VI as evaluation.

To compare two Dirichlet distributions, we utilize the log-likelihood ratio as the test statistic. Given two distributions corresponding to reference device / evaluation device pairs, denoted $\mathcal{D}_{\text{Evaluation}_1}^{\text{Reference}}$ and $\mathcal{D}_{\text{Evaluation}_2}^{\text{Reference}}$, we first join the data underlying these distributions to construct a joint distribution, $\mathcal{D}_{\text{Joint}}^{\text{Reference}} = (\mathcal{D}_{\text{Evaluation}_1}^{\text{Reference}}, \mathcal{D}_{\text{Evaluation}_2}^{\text{Reference}})$. Employing maximum likelihood estimation, we independently fit Dirichlet parameters to each individual device/evaluation pair and the joint, resulting in parameter vectors α^1 for $\mathcal{D}_{\text{Evaluation}_1}^{\text{Reference}}$ and α^2 for $\mathcal{D}_{\text{Evaluation}_2}^{\text{Reference}}$. Additionally, we fit a parameter vector α^{Joint} to the combined dataset. Finally, the log-likelihoods of each distribution, evaluated under their respective fitted parameters, are then computed. To quantify the difference between the two distributions, we calculate the following test statistic:

$$D = 2 \left[\log L(\mathcal{D}_{\text{Evaluation}_1}^{\text{Reference}}, \alpha^1) + \log L(\mathcal{D}_{\text{Evaluation}_2}^{\text{Reference}}, \alpha^2) - \log L(\mathcal{D}_{\text{Joint}}^{\text{Reference}}, \alpha^{\text{Joint}}) \right] \quad (7)$$

where $\log L$ represents the log-likelihood function. This statistic assesses the extent to which modeling the groups separately provides a better fit, compared to modeling the reference/evaluation device and the reference/reference device

together using a single Dirichlet distribution. Parameter estimation is carried out using maximum likelihood methods to ensure both convergence and robustness. This likelihood ratio test for independence thus evaluates whether the two Dirichlet-distributed evaluation/reference groups are likely to originate from the same underlying distribution or from distinct distributions. A value of D close to zero indicates that the two-distribution model does not substantially improve the fit over the single-distribution model, suggesting that a single Dirichlet distribution adequately describes the data. In such cases, there is insufficient evidence to justify the use of two separate distributions.

We present these likelihood ratios in Table V, indicating that especially the distributions $\mathcal{D}_{\text{Textile II}}^{\text{BTL II}}$ and $\mathcal{D}_{\text{Faros II}}^{\text{BTL II}}$ can be expressed as one distribution and are therefore closely related.

TABLE V: The likelihood ratios between two Dirichlet distributions of R-peak detection performance.

Phase	$\mathcal{D}_{\text{Textile II}}^{\text{BTL II}}$ $\mathcal{D}_{\text{Faros II}}^{\text{BTL II}}$	$\mathcal{D}_{\text{Textile I}}^{\text{BTL II}}$ $\mathcal{D}_{\text{BTL I}}^{\text{BTL II}}$	$\mathcal{D}_{\text{BTL I}}^{\text{BTL II}}$ $\mathcal{D}_{\text{BTL VI}}^{\text{BTL II}}$	$\mathcal{D}_{\text{BTL I}}^{\text{Faros II}}$ $\mathcal{D}_{\text{BTL VI}}^{\text{Faros II}}$
Sitting Relaxed	0.03	0.90	2.48	2.54
Sitting Video	0.19	3.84	8.52	7.49
Sitting <i>n</i> -back	0.04	0.49	6.36	5.58
Lying Back	0.12	1.64	9.73	10.51
Lying Side	0.21	1.96	1.08	1.61
Lying Side	1.19	8.87	5.96	5.08
Lying Stomach	0.27	4.10	10.02	10.96
Standing	0.26	5.40	6.49	5.97
Ergometer	0.15	0.93	0.25	0.23
Running	1.72	3.19	0.02	0.00
Walking	0.03	0.90	5.52	4.98

I. Training

To supplement our main article, we employed hyperparameter optimization using the TPESampler [15], tuning the learning rate within the range of 3×10^{-4} to 5×10^{-1} , a tree depth from 3 to 12, a number of estimators from 750 to 4000, and a gamma between 0 and 1.5. The model with the overall best hyperparameter of the inner folds was evaluated then evaluated on the outer test set.

REFERENCES

- [1] G. D. Clifford, F. Azuaje, and P. McSharry, Eds., *Advanced Methods and Tools for ECG Data Analysis*. Boston: Artech House, 2006.
- [2] U. Satija, B. Ramkumar, and M. S. Manikandan, "A Review of Signal Processing Techniques for Electrocardiogram Signal Quality Assessment," *IEEE Reviews in Biomedical Engineering*, vol. 11, 2018.
- [3] S. Luo and P. Johnston, "A review of electrocardiogram filtering," *Journal of Electrocardiology*, vol. 43, no. 6, Nov. 2010.
- [4] J. W. Mason, E. W. Hancock, and L. S. Gettes, "Recommendations for the Standardization and Interpretation of the Electrocardiogram: Part II: Electrocardiography Diagnostic Statement List: A Scientific Statement From the American Heart Association Electrocardiography and Arrhythmias Committee, Council on Clinical Cardiology; the American College of Cardiology Foundation; and the Heart Rhythm Society: *Endorsed by the International Society for Computerized Electrocardiology*," *Circulation*, vol. 115, no. 10, Mar. 2007.

- [5] P. S. Addison, "Wavelet transforms and the ECG: A review," *Physiological Measurement*, vol. 26, no. 5, Oct. 2005.
- [6] H. Li, G. Ditzler, J. Roveda, and A. Li, "DeScoD-ECG: Deep Score-Based Diffusion Model for ECG Baseline Wander and Noise Removal," *IEEE Journal of Biomedical and Health Informatics*, 2024.
- [7] M. P. Oppelt, M. Riehl, F. P. Kemeth, and J. Steffan, "Combining Scatter Transform and Deep Neural Networks for Multilabel Electrocardiogram Signal Classification," in *2020 Computing in Cardiology*. Rimini, Italy: IEEE, 2020.
- [8] J. Pan and W. J. Tompkins, "A Real-Time QRS Detection Algorithm," *IEEE Transactions on Biomedical Engineering*, vol. BME-32, no. 3, pp. 230–236, Mar. 1985.
- [9] G. B. Moody and R. G. Mark, "MIT-BIH Arrhythmia Database," 1992.
- [10] P. Hamilton, "Open source ECG analysis," in *Computers in Cardiology*. Memphis, TN, USA: IEEE, 2002, pp. 101–104.
- [11] T. Rodrigues, S. Samoutphonh, H. Silva, and A. Fred, "A Low-Complexity R-peak Detection Algorithm with Adaptive Thresholding for Wearable Devices," in *2020 25th International Conference on Pattern Recognition (ICPR)*. Milan, Italy: IEEE, Jan. 2021, pp. 1–8.
- [12] J. Emrich, A. Gargano, T. Koka, and M. Muma, "Physiology-Informed ECG Delineation Based on Peak Prominence," in *2024 32nd European Signal Processing Conference (EUSIPCO)*. Lyon, France: IEEE, Aug. 2024, pp. 1402–1406.
- [13] D. Makowski, T. Pham, Z. J. Lau, J. C. Brammer, F. Lespinasse, H. Pham, C. Schölzel, and S. H. A. Chen, "NeuroKit2: A Python toolbox for neurophysiological signal processing," *Behavior Research Methods*, vol. 53, no. 4, pp. 1689–1696, Aug. 2021.
- [14] T. P. Minka, "Estimating a Dirichlet distribution," 2012.
- [15] S. Watanabe, "Tree-Structured Parzen Estimator: Understanding Its Algorithm Components and Their Roles for Better Empirical Performance," May 2023.

Textile/Holter Dataset	
Dataset Signal Quality Evaluation	
Year of Creation 2023	
Instances Per Dataset 0 Public, 30 Private	
DOI https://doi.org/XXXXX	
Motivation	
Original Authors	Maximilian P. Oppelt et al.
Original Use Case	Device Quality Evaluation
Original Funding	Digital Health and Analytics, Fraunhofer IIS
Composition	
Sample or Complete	Private dataset
Missing Data	Some records with noise
Sensitive Information	Anonymized, no image/video data available
Collection	
Ethical Review	65_21 B on 16.03.2021
Ethics Committee	Friedrich-Alexander-University Erlangen-Nuremberg
Cleaning and Labeling	
Cleaning Done	2025-01-01
Labeling Done	2025-01-01
Uses and Distribution	
Notable Uses	Signal quality evaluation, difference in sex, projection, morphology
Other Uses	Classification of activity, psychophysiological cognitive load
Maintenance and Evolution	
Corrections or Erratum	None
Methods to Extend	None
Replicate Maintainers	Maximilian P. Oppelt
Breakdown	
Physiological Measurements	Electrocardiography (ECG) lead I, II, V1 BTL, lead II Faros and I, II from wearable garment
Demographics	Age, sex
Body measurements	Height, weight, upper body width, shoulder width, relative electrode positioning, upper body hairiness
Ergonomics	Quality of fit

Fig. 1. A data card styled after nutrition labels. Description of wearable textile ECG garment.